MSc thesis in Sustainable Energy Technology

# Dynamic Modelling of Wind Loading on Floating PV Systems

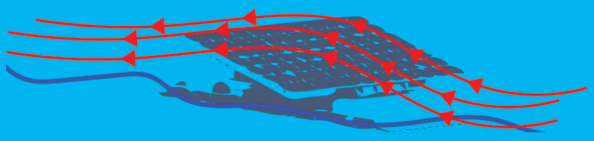

Aalif Mohammed
2024

TU Delft

**MSc thesis in Sustainable Energy Technologies**

# Dynamic Modelling of Wind Loads on Offshore Floating PV Modules

Aalif Mohammed

To be publicly defended on 29 August 2024.

A thesis submitted to the Delft University of Technology in partial fulfillment of the requirements for the degree of Master of Science in Sustainable Energy Technology.

Aalif Mohammed: *Dynamic Modelling of Wind Loads on Offshore Floating PV Modules* (2024)

The work in this thesis was carried out in the:

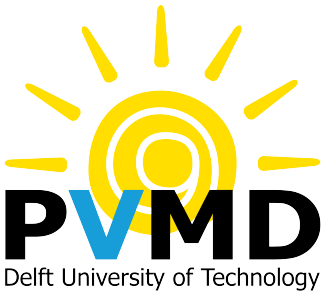


Photovoltaic Materials and Devices research group
Delft University of Technology

| | |
|---|---|
| Student No : | 5767571 |
| Project duration : | Jan 2024 - August 2024 (32 weeks) |
| Supervisors: | Dr . Rudi Santbergen<br>*Assistant Professor (ESE / PVMD)* |
| | ir . Sathya Shanka Vasuki<br>*PhD student (PVMD)* |
| Thesis Committee : | Dr. Rene van Swaaij<br>*Associate Professor (ESE/PVMD)* |
| | Dr. Mohamad Ghaffarian Niasar<br>*Assistant Professor (ESE/ High Voltage Technologies)* |

# Abstract

As the global community seeks to improve current energy technologies for a sustainable future, offshore PV systems show great potential to overcome the land use limitations of traditional PV systems. There is a complex interaction between different environmental forces at sea with the PV structure. Empirical studies on these environmental interactions can provide critical insights to optimize the design of offshore PV systems. This thesis has identified a gap in wind loading studies on offshore PV designs. The primary objective of this research is to develop a methodological approach for studying the wind-induced tilt variations in floating PV (FPV) systems, with the intent of informing future PV performance assessment frameworks. A numerical modelling approach using the CFD tool ANSYS Fluent is adopted as the base methodology. The first phase of the study employs single-phase wind tunnel models in 2D and 3D to study flow behaviour over the required geometry. The models are validated against literature and used as the basis to construct a multi-phase model to simulate wind flow over a floating body and how it moves in response to the water surface.

The model is used to perform sensitivity studies on wind speed, module orientation, module tilt, and floater height. The simulation results indicate that tilt variations induced by wind flow are minimal, under 5°, for still water conditions. In addition, it also suggests an increase in wind velocity increases the non-linearity in the rotational response of the body, changes in the direction of rotation depending on the speed of the flow and tilt of the module, and a sharp increase in rotation with an increase in floater height. The highest rotational response of 4.07° (anticlockwise) was observed for a design tilt of 24° and a wind speed of 40 m/s.

Based on the simulation results, a PV yield assessment is done, and it is found that the inclusion of tilt effects changes the yield by less than 0.5%. Given the high computational cost involved, a numerical approach for wind load evaluation is not justified in terms of yield variation. For future work, it is recommended to first conduct experimental studies to verify the effects of wind loading on different FPV system designs. This could be supplemented with numerical approaches in the future using high-performance computational resources.

# Acknowledgements

The work done in this thesis is the amalgamation of several months of effort combined with a lot of help from my family, friends, and supervisors. I'd like to express my gratitude to them. To Sathya, thank you for giving me the opportunity to work on this project. I wanted to work with something related to water when I came here and this managed to be that. To Rudi, thank you for calming me and guiding me in the process of the thesis when I was nervous. It felt relieving that despite anything, I was assured that with a coherent narrative, I'd have a good thesis at hand by the end of the process. Also, I'd like to thank Rene and Mohamed for agreeing to be part of my defense committee, it was a late request and I am thankful for your presence. I also have to thank Alba for her research on the tilt models for the FPV and for helping me with the weather data from KNMI and other suggestions regarding approaching this work. This thesis really wouldn't be what it is, if it weren't for your contribution.

Some names I have to specifically thank in TU Delft are Sakshi and Naajein. They were rock solid in their support at several points in the thesis period and were hugely motivational for me to proceed with the work no matter how stuck I was. Thank you for being there during this period. To the people in the Palestinian camp at TU Delft, it was during this research period that I met so many of you and got to be part of the wonderful community of resistance. It was lovely to be part of something political in a technical university. Helps you put things in perspective and think about the socio-political aspects of technology as well. Love to the intifada! Free Palestine! To my parents and my sister who constantly checked up on me during this process and trusted me to do a master's abroad after living my whole life in Trivandrum, thank you for your unwavering support.

Finally, I have to thank my lovely partner, Krishna, who has been a ray of sunshine throughout the thesis. You have been the sounding board for every idea for this work and honestly know my thesis better than my supervisors do at this point. It's been lovely to bounce ideas with you because sometimes I trust your academic instinct more. This thesis is as much yours as it is mine. But not just academically, it's been a lovely year to spend with you and I can't wait for you to draw a graduation hat on the picture you have at home once this is all done.

*Aalif Mohammed*
*Delft, August 2024*

# Contents

# List of Figures

# List of Tables

# 1 Introduction

> ”We cannot solve our problems with the same thinking we used when we created them.” *Albert Einstein*

## 1.1 Global Energy Context

Energy is something we require in modern civilization to power our daily needs. The electronic devices used to write and read this report exemplify how important this is. Energy extraction and usage in the present day mainly come from utilizing fossil fuels. From the climate report by Ember, Global Electricity Review 2023 [18], we see the actual percentage of fossil fuel utilisation to be around 61%. Due to $CO_2$ emissions and polluting $NO_x$ emissions, which exacerbate global warming, there have been concerns since the late 1950s [19] about the usage of fossil fuels for energy [20]. There has been a steady rise in sea levels [21] and climate change [22, 23] in the years preceding that has caused the energy industry to take these concerns more seriously [24].

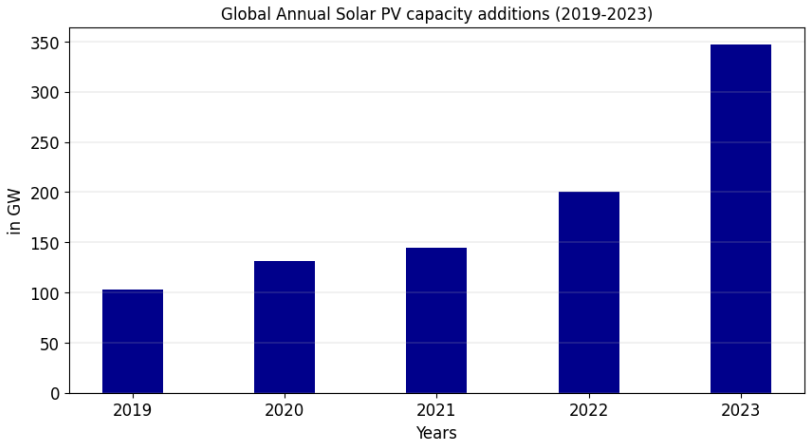


Figure 1.1: Solar capacity growth from 2019- 2023, data from IRENA [1].

The transition of the energy industry from fossil fuels is backed by the development of new technologies that utilize renewable energy. Global investment in renewables as of 2023 is 1740 billion USD and makes up a little more than 60% of the total energy investments [25]. The most popular options currently being globally pursued are solar and wind energy, out of which solar energy has the most expansion potential and global investment backing it. Figure 1.1 shows the global solar capacity addition plot in recent years and it can be seen that it is increasing each year. Particularly, the capacity additions in 2023 are 75% more than that of 2022. Based on international climate policies adopted, this value is only going to increase. It becomes important therefore to consider the limitations of this energy source that will arise in the future. Some of the main issues that limit the use of solar energy worldwide are its material-intensive production methods [26] and their high land area usage [27, 28].

Understanding the context of this change also necessitates a look into the future, like in 2050 when our population would be 9.7 billion [29]. The annual electricity generation would be expected to be $30-76\%$ more than today's energy requirement according to the U.S Energy Information Administration [30]. In the case of the Netherlands, the electricity demand would increase by $180-250\%$ that of 2019. To fulfil electricity requirements in 2050, it is estimated that around 70 TWh/yr or 80 GWp of solar PV would need to be installed [31, 32]. From Figure1.2, it would imply that land use of around $10^5$ hectares is to be expected [2]. With the large scale of installation required, considering only ground-mounted PV would be spatially constraining and expensive [33].

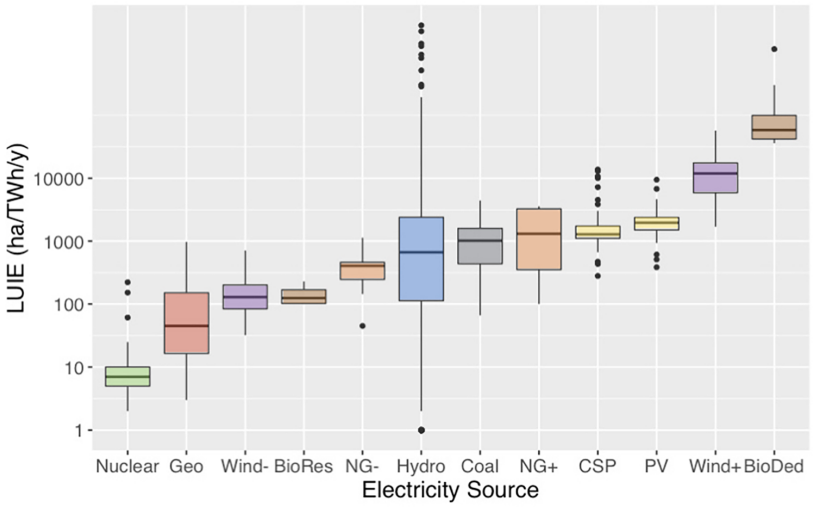


Figure 1.2: Log plot comparison of land use requirements for different energy sources [2].

That introduces the question, what other surfaces can we install solar panels on? Quax *et al.* [34] mentions several different Land Use and Water Types (LUWT) to incorporate solar panels. It lists dwellings, service sector buildings, industries, and green areas as possible options on land. On the water surface, the options for PV installation are canal-top systems, reservoir/lake-based systems, and offshore installations. Different surfaces offer a separate set of challenges for PV system design. For example, for PV on land, the focus would be to

use existing mature technologies that are cheap to install, whereas for PV on water surfaces it becomes important to know if PV is lightweight and if it performs well in highly humid conditions among other things. It becomes important therefore to choose appropriate PV technologies for the particular use case.

## 1.2 Context in the Netherlands

The development of PV systems in the Netherlands is in tandem with the National Climate Agreement for 2030 [35]. In the agreement, the Netherlands aims to generate a total of 84 TWh of sustainable electricity, 35 TWh on land, and 49 TWh at sea. The energy at sea is proposed to come from offshore wind projects in the North Sea mainly. The major designated wind farms are the Hollandse Kust (noord, zuid and west) and the Ijmuiden Ver areas with over 10 GW of capacity combined [36].

In addition to offshore wind turbines, there has been increasing interest in developing floating solar farms near offshore wind farms. There are advantages to pursuing such hybrid systems in terms of energy yield per unit area and stable energy supply. One notable technical advantage in this scenario would be utilizing the installed cabling systems of the wind turbines for solar farms as well. Such cable pooling systems are found to be economically advantageous [37] and technically efficient for the complementary generation patterns of solar and wind energy in the North Sea.

The environmental conditions in the North Sea, however, pose significant challenges for the deployment of offshore PV. The main challenges to overcome are the wind and wave loading on the PV panels. In the southern North Sea, significant wave heights as high as 14.2 m can be expected while no obstructions around the solar panels can result in sustained winds of more than 35 m/s [38].

Due to the nascent nature of the field, there is a lack of long-term field data to study the behaviour of floating PV installations. Studies in the field of operational behaviour especially under environmental loading are necessary to understand what we can expect from FPV systems.

## 1.3 Floating Photovoltaics

A floating photovoltaic installation is an attempt to utilize the vast area of water bodies around the world to generate energy. The main challenge of an FPV system is to replicate the performance of land-based PV systems while also including floating body effects. Five main system components help to make this possible. These are the PV module, inverters, floaters, system frame, and mooring system. These are discussed briefly below. An illustration of an FPV system is shown in Figure 1.3 which contains the different system components.

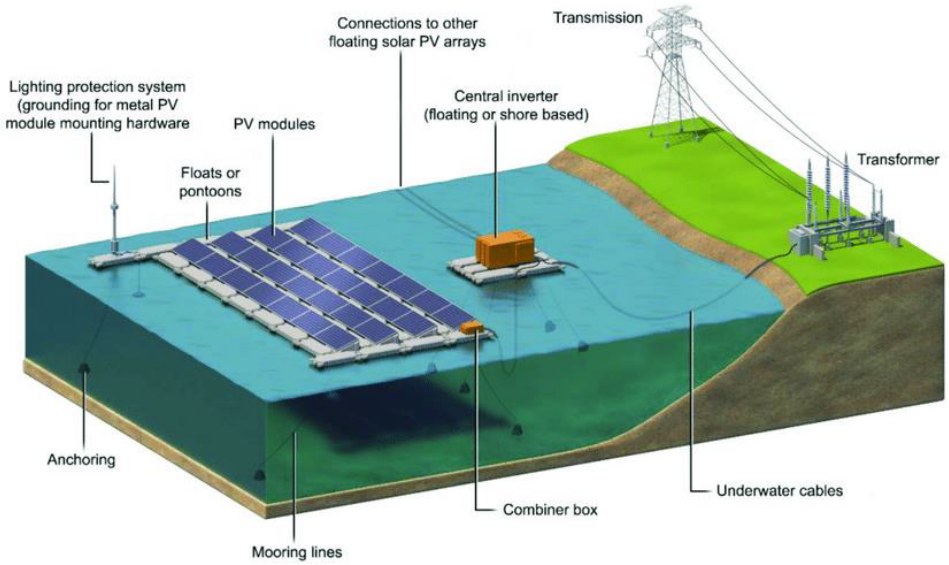


Figure 1.3: Illustration of a floating photovoltaic system [3].

- **PV module**: PV modules are the most important part of the device and inform the gross energy yield of the system. These modules are usually rigid crystalline silicon modules although flexible thin-film cells are also in development [39, 5]. Apart from the endurance tests for land-based PV, it is recommended to consider load testing for wind and wave loading and to conduct corrosion tests for salts and ammonia for the selection of offshore PV modules [40].

- **Inverters**: Inverters help regulate the current obtained from the solar farms and transport current onshore or to the grid. The choice of inverter depends on the site characteristics and the layout of the solar farm chosen [41]. Generally, floating solar systems use string or central inverters with micro-inverters also being used for small installations. For larger systems, it is recommended to use central inverters and transformers on separate floating structures [41, 40].

- **Floaters**: The floaters provide the necessary buoyancy for the systems to stay afloat. They are usually cubic, pontoon-shaped, or tubular and made of plastics like HDPE, MDPE, PVC, or styrofoam [5]. The floaters should ideally handle at least the load of the system frame, the panel, the electrical equipment, the cabling, environmental loads, and human load during maintenance [42].

- **Support structure**: This is the main structural component of the system that is on top of the floater and helps hold the panel in place. The design of the system frame depends on the type of floater used. It can range from a simple plastic bracket to a steel structure with struts. The frame must be structurally stable to protect the module under different environmental loading [43].

- **Mooring system**: Mooring cables are attached to the system frame to anchor the installation. They help dampen the system response to environmental loading. The type and number of mooring lines used depend on the FPV type and system layout. Generally, it is preferred not to use too many mooring lines in a system. This is because, although they help with damping, they also increase the cost of the system and the complexity of movement of the system under load [4].


Figure 1.4: An overview of the installed FPV technologies from 2007-2014 [4].

### 1.3.1 Current state of FPV installations

FPV systems are categorised into three types based on their site of installation [44].

1. Lake/reservoir systems
2. Canal top systems
3. Offshore systems

FPV installations in the current energy landscape are mainly catered towards the first two inland water systems or near-shore coastal FPV installations. [45].

One of the first FPV projects to be installed is a 20 kW pontoon-type installation in Atachi, Japan [46]. Several small-scale floating photovoltaic systems were installed over the next 5 years in Spain, Japan, South Korea, Italy, and the USA. Figure 1.4 shows an overview of the installed technologies until 2014 [4]. The FPV systems were deployed in reservoirs and lakes with the main attraction being alternate land use opportunities, curbing evaporative losses, and higher efficiencies due to better cooling of the panel. Some notable examples are the installation by Ciel et Terre in Piolenc, France, with their product Hydrelio [47] and the projects by SCINTEC in Italy which included solar tracking in the floating modules.

However, it was only after 2015, that inland FPV reached a state of commercialisation. These installations were mainly done in Japan, Singapore, Korea, and China. Of these installations, the 5 MW installation in Johor Strait by Sunseap is a notable first major installation [48]. There have been several such installations since in Asia with Ciel et Terre being the leader with a total of 1.6 GWp installed till now [49]. Both Sunseap and Ciel et Terre who have made these massive installations employ similar FPV designs with High Density Polyethylene (HDPE) pontoons that contain the solar panel in a bracket. Figure 1.5 shows this design installed in the Hyogo Prefecture in Japan.

Figure 1.5: Picture of a HDPE pontoon floater design commonly used for large inland FPV systems

Offshore PV has not been tested out on a commercial scale as of yet. Several companies like OceansofEnergy, OceanSun, Bluewater and Solarduck offer novel solutions for applications in marine environments. They are at varying Technological Readiness Levels (TRL) with Swimsol in Austria and OceanSun in Norway offering market-ready solutions for wave exposure conditions in the range of 3-6 m [50]. Oceans of Energy was the first company to test offshore floating solar under sea conditions with a 50 kW pilot in 2019. This was a collaboration with several Dutch companies as a part of the *Zon op Zee* project [50, 51]. They are also heading the first commercial hybrid FPV project in the North Sea in between the offshore wind turbines of Hollandse Kust Noord wind park which is a 0.5 MW installation [51].

### 1.3.2 Floating PV performance

FPV systems, although using the same operating principle, have a unique set of challenges compared to their land-based counterparts. Apart from the set of components described in Section 1.3, technical challenges also arise in its electricity generation capabilities. This could be due to its location, the PV panel orientation and layout, environmental conditions, or other phenomena [41]. Several manuals exist describing the technical challenges involved in floating solar design and development [40, 45]. From this literature, the most relevant actors affecting the PV yield are determined as:

- **Temperature:** The effect of the water surface on the temperature and yield of an FPV module has been researched using Computational Fluid dynamics (CFD) studies [52], experimental studies [53], and mathematical models [54]. Lower temperatures in sea conditions are generally favourable to electricity generation in PV modules. It is found that in the summer months, around $5-10\%$ more yield than land-based PV can be expected in the Netherlands [4].
- **Absorbtion and reflection losses:** Since the sea has a different albedo and humidity as compared to land, the general balance of absorbed and reflected light on the module varies. This changes the diffuse and reflected components of irradiation available for a PV module [4, 55]. This effect is further influenced by panel layout, sun position, waves, and winds and is a complex phenomenon that can be very difficult to model.
- **Module degradation:** Water composition, salinity, turbidity, and atmospheric humidity differences will also cause the module to corrode and degrade faster than their land-based counterparts. This negatively affects PV yield and appropriate material considerations and design considerations should be made [12, 45].
- **Panel Movement**: PV tilt and azimuth determine how much solar power is available at any instant. Tilt and azimuth may shift due to environmental effects such as wind, waves, or ocean currents [43]. This can affect PV yield and inverter efficiency due to fluctuating power output. Hence, it is advantageous to understand the motion of the panel in response to the weather conditions. There are several studies [11] [56] [57] currently being done for wave-related effects on panel movement. A study by Golroodbari *et al.* [54] suggests an averaged PV tilt under 10°due to wave interactions.

## 1.4 Research Gap and Scope

The PVMD group at TU Delft aims to build expertise in the design and performance of solar cells, modules, and systems. Offshore solar as a novel technology has not been commercially tested yet and we do not yet know how the environmental conditions affect its performance. From literature studies [11, 43], panel tilt and azimuth changes in response to environmental effects are found to be important aspects affecting FPV performance. While panel movement due to wave interaction is being studied currently, a research gap is identified in the study of

panel tilt and azimuth variations due to wind interactions. This makes a reliable methodology incorporating wind effects in the operation and performance of the system to be beneficial.

***This work aims to devise a methodology to calculate the tilt variation of offshore PV and check the suitability of this approach for FPV performance assessment.***

The work will mainly concentrate on the tilt variation of a PV module under a normal wind profile. It will assume rigid body conditions and not consider the performance under extreme environments. The study also assumes no wind-induced wave interactions or situations where the structural stability of the module is compromised. These may be in the form of breakage, degradation, toppling, etc.

## 1.5 Research Questions

Based on the literature researched on the topic of floating solar systems, it has become evident that there has been no methodology for assessing the change in tilt and azimuth of floating PV panels to wind loading. Therefore, the primary focus of the work will be to perform dynamic wind load analysis on FPV for an offshore PV installation and analyse the tilt variations. Critical parameters will be analyzed to answer the following questions:

1. What is the methodology chosen for evaluating wind loading on offshore floating PV?
    - *What are the relevant FPV geometries that are used for floating solar installations?*
    - *What are the different methodologies for assessing wind response of floating PV?*
2. What is the wind flow behaviour around a PV module?
    - *How do the flow characteristics change with the addition of floater geometry on the panel?*
3. What is the tilt variation of an FPV module exposed to wind?
    - *What are the most important CFD model settings that are critical to this problem?*
    - *What is the tilt variation of the module in response to different geometric and flow parameters?*
4. Is the methodology used in this thesis beneficial to assess FPV performance? If so, what further work is required?

# 2 Literature Study

This chapter introduces the different FPV archetypes i.e base types and the work done in analysing wind effects on PV. Firstly, a classification is done for various rigid-body FPV installations based on the nature of the floaters used. Then, existing literature on tools used for wind loading on solar panels will be reviewed in the next section. This will be followed by a literature review of the studies done on environmental loading on floating PV systems. Finally, based on the literature review, the first research question on the choice of methodology for evaluating wind loading on offshore floating PV will be answered.

## 2.1 FPV types and classification

Floating photovoltaics is an emerging technology and there is no clear design that is advantageous. This results in various companies proposing their unique designs for the floating structures. The FPV classifications described here will cover rigid-body FPV types using c-Si modules. This means that thin-film technologies and other flexible floating photovoltaics will not be discussed. Based on the historical installations, there are three main archetypes found advantageous to distinguish based on floater geometry. This classification is a modified version based on the work by Cazzaniga [5] and Huang *et al.* [48] and is discussed below.

Figure 2.1: Tubular float system installed by Terra Moretti [5].

1. **Tubular float systems:** These are the most commonly used FPV archetype. They use floating tubes with metal structures (aluminum or steel components) as their framework. A common example of this structure is the FPV installation by Terra Moretti in the Suverto project as shown in Figure 2.1. This type of PV archetype is characterized by its simple, low-cost construction and is suitable for freshwater bodies.

   Suitability for offshore conditions for tubular floats is yet to be determined as there are no major installations (>1 MW) has been found in the literature. Points of concern for the technology are the stress failure of the nodal connections to the float, the structural stability under environmental loads, and the cost of construction of maintenance platforms in large installations. A notable system of this type called "Gable Slender" [5], which eliminates some of the issues relating to stability but it is not yet certain what other issues might arise as these systems are not tested.

Figure 2.2: Individual raft-based PV at Okegawa via Ciel et Terre [6].

2. **Individual raft systems:** Individual HDPE (High-Density Polyethylene) and MDPE (Medium Density Polyethylene) rafts are used in these systems to attach PV modules with hooks or hinges. Each PV has a floater and this type of system does not generally have struts. Due to ease of construction and installation, raft-type systems have been the most commonly used technology for major installations. Ciel et Terre is the a very popular floating solar company installing individual raft type geometry [49]. Their product, Hydrelio, is shown in Figure 2.2.

   Despite the ease of construction, these types of modules are difficult to install in offshore conditions due to the complex mooring system arrangements to be made for securing the platform [5]. Since every module is lightweight and subject to environmental loading, its stability is also questionable. Further wind and wave loading testing is required to determine usability in offshore conditions.

Figure 2.3: Pilot installation by Oceans of Energy in the North Sea [7].

3. **Platformed surfaces:** The PV panels are laid down flat on a platform or a membrane supported with the help of buoys arranged around the floating frame. The panels are normally flat but can be designed to be inclined. These structures are much more structurally stable as the panels are grouped under a single pontoon. However, the size of the platform/membrane will be limited so it is necessary to find proper arrangements to deploy these systems properly.

   This classification includes cubic buoy-supported installations in steel platforms and recently introduced offshore floating PV technology like that by *Oceans of Energy* as shown in Figure 2.3. The technology is still in its nascent stage and has to be tested for the potential for large offshore installations [7].

## 2.2 Wind loading on offshore PV

One of the main challenges with the installation of offshore PV systems lies in dealing with environmental loads [41, 40]. A module deployed in open sea conditions can face three major types of loads: due to wind, waves, and currents. Other factors might affect PV performance as well such as collision loads from other objects at sea, droppings from birds, etc. However, this type of effect is quite random and is considered out of scope for this work.

The focus of this work will be on wind loading in FPV installations. This section will provide an outlook on the existing techniques used to evaluate wind loads on PV panels. The study was not limited to floating PV, as it is still an emerging field with no long-term usable data useful for wind loading analysis. Instead, analysis techniques for PV on land are first investigated to understand how wind load analysis can be approached for the offshore case study.

### 2.2.1 Existing methods for wind loading

Wind load design for PV started as an extension of wind load standards for buildings. They are described differently in different regions by building standards such as Eurocode, ASCE7, and JIS [58, 59]. Drag, lift, pressure, and overturning moment are the most important forces considered for wind loading. Wind load design is focused on finding the mean and peak force coefficients on the solar panels which would help determine the failure limit states of the module [60]. Large-scale field tests are usually not viable for the evaluation of these coefficients, so computational fluid dynamic (CFD) calculations and lab testing on scaled models were found to be reliable for evaluating wind loading. CFD studies were used mainly as an investigative tool while the wind load design of PV modules was validated by lab tests in wind tunnels and torque tubes [61, 62, 63, 64].

A good classification of the methodologies [8] currently used to evaluate wind loading is shown in Figure 2.4.

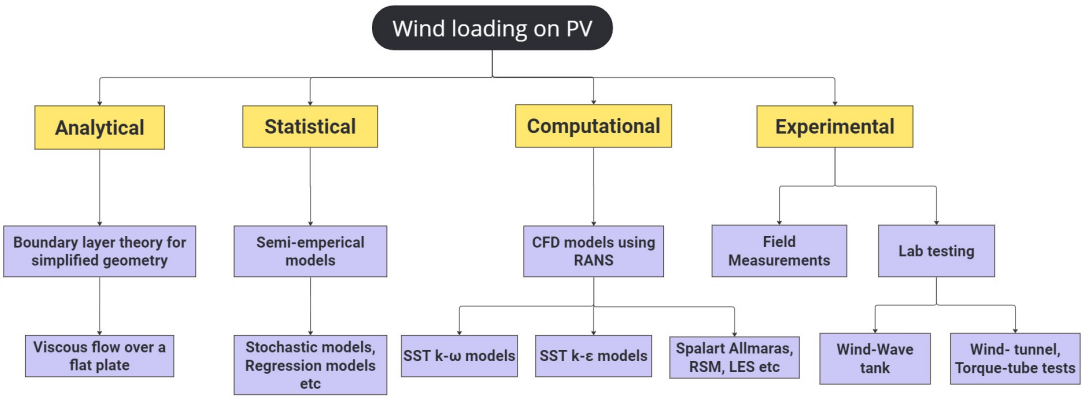


Figure 2.4: Classification of different methodologies to evaluate wind loading [8].

Out of the methodologies mentioned in Figure 2.4, computing forces on a floating PV panel would be exhaustive and require geometric simplification for static analysis. However, for a moving body, this task becomes virtually impossible. It could provide base results for calculation but would fail to provide accurate results considering the complexity of geometry and flow. Semi-empirical studies of wind loading on offshore panels depend on pre-existing force coefficients from previously existing engineering standards on land [43]. In the absence of experimental data available and for new technologies that have not yet been commercially deployed, the most reliable methodology thus becomes computational evaluation. A decision matrix of the same is shown in Table 2.1.

| Method | Complexity | Accuracy | Data availability |
|---|---|---|---|
| Analytical | High | High | No analytical studies done |
| Statistical | Low | Sufficient | Data available only for land-based PV[43] |
| Computational | Affordable | Sufficient | Prior CFD studies available for reference |
| Experimental | Affordable | High | No experimental studies available |

Table 2.1: Decision matrix to determine a feasible method for wind load analysis of a floating PV.

### 2.2.2 Computational evaluation of wind load

Computational methods used for wind load analysis utilize simplified numerical solutions of the Navier-Stokes equations [65]. These equations are employed in finite-volume computational methods to solve steady-state and unsteady conditions of CFD problems. For high Reynolds number flows, turbulence models help to depict flow characteristics depending on the application and the analysis required [66].

Reynolds Averaged Navier Stokes (RANS) models are simplified turbulence models that are computationally affordable and suited for low-intensity turbulence. In industrial flow problems, RANS models are the most commonly used to compute flow solutions [65]. Large Eddy Simulations (LES) and Detached Eddy Simulations (DES) are typically used for accurately simulating turbulent flow behavior, especially for high-intensity turbulence [61, 67]. The most commonly used turbulence models for CFD applications are the SST $k-\omega$ and the $k-\varepsilon$ models. These are variations of the RANS models which use turbulence viscosity and dissipation in energy to calculate stress-strain relations in turbulent flow [66].

This thesis will assign two broad categories to the analysis done in the field of wind loading on solar panels, namely load analysis and flow analysis. Load analysis refers to the study of drag, lift, pressure, and moment acting on the solar panel. In contrast, flow analysis refers to studying flow characteristics such as turbulence, flow separation, vortex shedding effects, etc. For both kinds of analysis, certain parametric variations such as tilt variation, ground clearance, and wind speed are commonly used to study the behaviour of the system.

The work done by Jubayer *et al.* [9] is an example of load analysis being done on PV panels. Wind flow over a solar panel is investigated as shown in Figure 2.5. This particular study uses the software OpenFOAM to construct a 3D unsteady RANS model to investigate the pressure coefficients in a panel subjected to wind loading. It is one of the first instances of computational evaluation of wind loading on a PV array and investigates the effect of the Reynolds number of flow on the system. Critical geometrical parameters for wind load such as the angle of inclination of the panel and row and column spacing between the panels have been analyzed using this type of analysis [68].

Flow analysis requires much more accurate turbulence models and is a bit more computationally intensive. However, it also provides a much clearer picture of system behavior and the

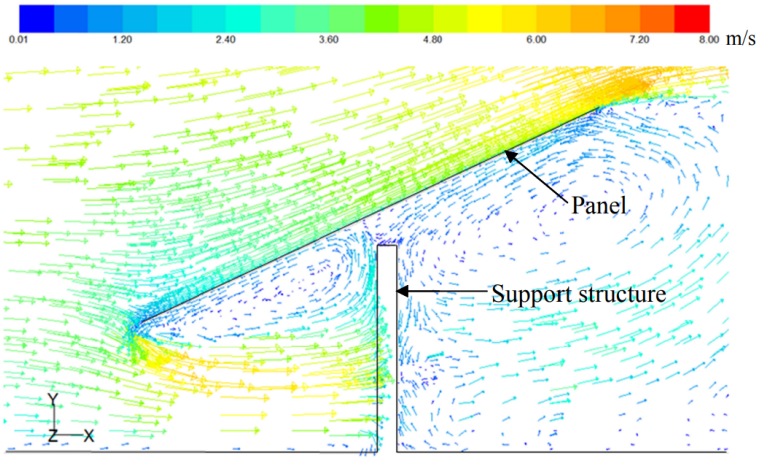


Figure 2.5: CFD velocity contour around a solar panel from [9].

changes caused by variations of geometric parameters [69]. Flow analysis is usually computationally limited to the study of local effects around the panel as the high accuracy requires sufficient computational demand as well. In the numerical investigation done by Shademan *et al.*, [69], there is a certain amount of attention done to the meshing to accurately model flow effects rather than focus on the turbulence model. This is effective when a large number of different parametric analyses are to be run and the computational resources need to be efficiently used.

Since the simulation of the movement of FPV panels in water is a novel study, it becomes important to pay attention to both analysis types and follow a hybrid approach. Results from flow analysis will be useful to describe the flow effects that lead to movement, while force analysis will be useful in quantifying this effect and providing numerically valuable results.

### 2.2.3 Analysis of environmental loading in floating PV

There is no comprehensive methodology as of yet for the analysis of dynamic wind loading conditions for offshore PV systems. However, several studies to evaluate the structural stability of FPV systems have been conducted [70, 71, 43]. Many of these studies focus on wind and wave analysis with significance given to the latter loading as it is much more prominent. However, extreme events leading to damaged floating PV systems [72] have prompted investigations on the effect of wind on floating panels as well.

Structural effects are usually analyzed with FEM software [70, 71] or analytically [43]. The studies determine how the wind loading causes stress and failure on the structure but the methodology used is not well documented nor is it clear what the behavior of the system is. Mursid *et al.* [10] investigates a structural study on raft-based systems affected by wind, wave, and current loading using SolidWorks non-linear solver. The stress distribution and maximum allowable stress on the floater are analysed with existing ISO standards for LDPE

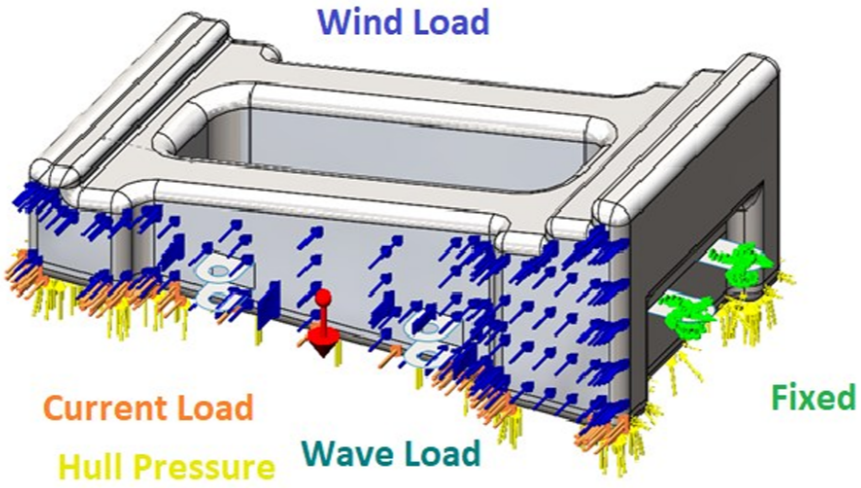


Figure 2.6: Wind Wave and Current loading on the floater as a free body diagram [10].

and the conclusion is that the forces exert stresses lesser than the allowable stress of the raft material. However, here the loads are just applied as uniformly distributed loads across the floater as in Figure 2.6, and the forces computed are based on IALA (International Association of Lighthouse Authorities) design standards for general marine structures. It is evident from previously done tests on solar panels that UDL (uniformly distributed load) cannot be applied to this structure [62] and static force applications can be misleading [63]. This implies that these results have to be rechecked and validated from actual tests run on floating systems with panels. A similar structural evaluation study was done by Kim *et al.* [73] for platformed systems with FRP members where they used Korean building standards on land for structural evaluation.

CFD studies have also been used to improve the validity of structural stability assessments as they provide an approximation of system interaction as well. Popular CFD studies have been carried out using ANSYS Fluent and OpenFOAM. Fluid-structure interaction is done using tools like ANSYS AQWA and ADINA. The usage of ANSYS Fluent and AQWA together is identified as a popular way of analysing both of these effects. Lee *et al.* [74] have done a 2D CFD study using Fluent on a platformed FPV installation, wherein the aerodynamic coefficients from the study and how it varies from the ones used in the fisheries and harbour design guidelines in Korea are analysed. The results showed that the design guidelines overestimated the wind load coefficients but this could be because 3D effects and turbulence effects were not properly considered in this study. Also in addition, there is not much information on the system behaviour itself as the loads are static.

Joo *et al.* [56] has a different approach to evaluating wind loading on floating PV. A flow analysis is performed to determine the wind loading on the system. This considers the geometry of the system and does not just relate the forces as proportional to the exposed area as proposed by current design standards. Also, the study was performed for an array and not singular modules. The study interestingly shows different results than previous papers in terms

of loading on various panels. The general trend of drag or lift seems not to be decreasing but to be fluctuating across PV rows. Thus the wind load design in this paper considers modules in the front of the array and the center as the most vulnerable. Since it is a newer paper, this research needs supplementary evidence.

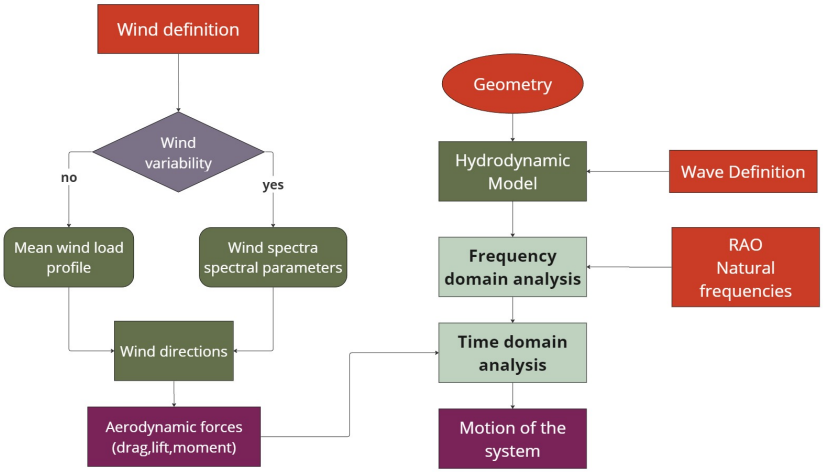


Figure 2.7: Methodology for determining the dynamic response of a floating PV structure [11].

Apart from the studies for structural stability, different methodologies for load evaluation are also investigated in literature [72, 11, 75, 8]. Honaryar *et al.* [8] utilise the DNV guidelines to provide direct wind load on an individual raft-type FPV. The study simulated wind-induced wave effects using the Volume of Fluid (VoF) model in the ANSYS CFX solver. So, it is a semi-empirical+numerical approach that was followed to simulate wave effects along with wind loading.

Choi *et al.* [11] describe a much more comprehensive approach to finding the dynamic response of an FPV structure and determining structural stability. The study brings into focus the nature of the analysis for wind and wave loading and discusses the coupling of numerical solutions for both. Wind loading is determined as a time-domain analysis while wave loading is a frequency-domain analysis as in Figure 2.7 for a tubular-float type FPV. Here, wind loading is determined analytically using force coefficients for drag and lift. Similar studies for yield determination also utilise analytical force coefficients to determine wind loading in hydrodynamic analysis [54]. Numerical studies still need to be done therefore to determine wind force on floating panels and how it varies based on wind behaviour and panel geometry.

### 2.2.4 CFD Methodology for this work

Figure 2.8 shows the workflow chosen and followed in this thesis work. Initially, the PV panel geometry is defined. This involves defining the physical dimensions of the body and the numerical evaluation points of a mesh. The wind profile is then defined for the flow analysis

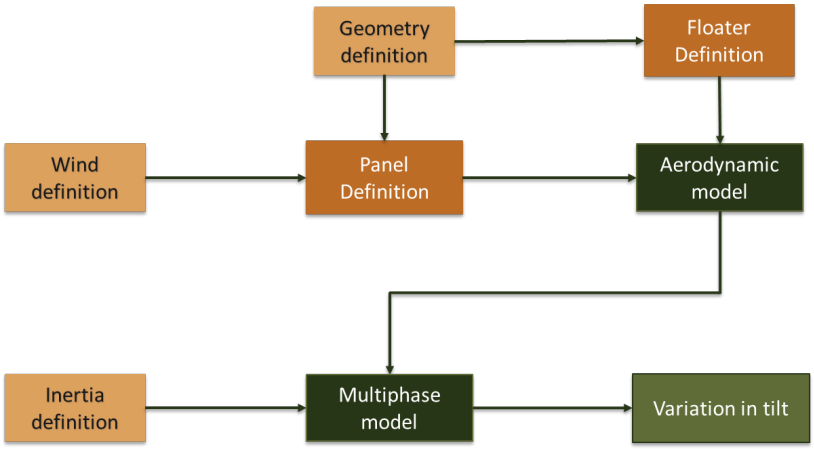


Figure 2.8: Workflow for the simulation model used in this thesis

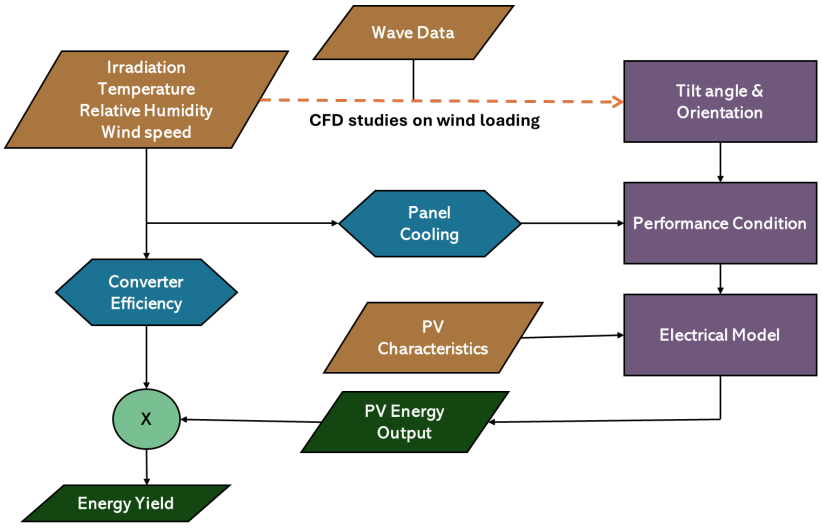


Figure 2.9: Modified workflow of FPV energy yield modelling [4].

around the body. This forms the basis of the aerodynamic model used to investigate the wind flow around the device. Once this model is validated, the geometry will be modified to a simplified individual raft-type FPV and the flow behaviour and the forces acting on the module will again be evaluated. Once there is an idea of the flow behaviour around this geometry, a multi-phase (air-water) model will be constructed with the same wind flow conditions and the body will be given inertial characteristics. The rotational movement of this body will then be recorded and used to assess the tilt variation under different wind conditions.

Figure 2.9 shows a modified workflow of the FPV yield modelling done by Golroodbari *et al.* [4]. The modified workflow would consider panel movement due to wind as an additional factor. The results from the CFD analysis could be used to supplement the FPV yield assessment model by working in combination with models predicting wave-induced motion.

## 2.3 Summary

This chapter discusses the study of wind loading on floating solar panels. The study of the effect of wind on the movement of floating devices is found to be a novel research topic. The following research questions from Section 1.5 are answered.

**What is the methodology chosen for evaluating wind loading on offshore floating PV?**

The study of wind loading on offshore floating PV requires quantitative assessment, and no experimental methods or previous work are available, a numerical approach is proposed as the evaluation methodology. Contemporary studies on floating PV panels are reviewed and used to formulate a methodology for this approach. A simplified methodology is then derived from a wind and wave load analysis study done by Choi *et al* .[11].

*What are the relevant FPV geometries that are used for floating solar installations?*

FPV designs with the potential for offshore deployment are classified into three different archetypes [5] [48]. The archetypes are named tubular float, individual raft, and platformed systems.

*What are the different tools for assessing wind response of floating PV?*

The tools available are analytical, statistical, computational, and experimental. Analytical solutions are found to be too complex and unsuitable for the scope of this study while there is no long-term data to create empirical fits for wind loading. CFD tools are found to be much more suitable in the assessment of floating systems in the absence of statistical and experimental data.

# 3 Single-Phase Flow

The initial solution approach chosen to analyze wind loading on the floating PV panel will be discussed in this chapter. The chapter will consist of static flow setups which are used to understand wind flow around PV panel geometry and FPV module geometry. The pre-processing of the CFD models will be discussed initially. Then, a section will be devoted to understanding transient flow around a flat plate using a 2D and a 3D model which is validated against literature. The final section of the chapter will briefly describe the characteristics of the flow around an individual floater-type FPV geometry in 2D. The flow characteristics observed will help understand the wind loading on the FPV device. This information will be used to answer the second research question regarding the wind flow behaviour around a PV module and how it changes with the addition of a floater geometry.

## 3.1 Aerodynamic Model Setup

Following the methodology from Chapter 2, firstly an aerodynamic model of a PV panel is created to investigate single-phase flow around a panel. The flow behaviour and the forces acting on the flow help us understand the wind loading on a PV module. The following sections describe the steps taken to define the problem.

### 3.1.1 Defining the flow field

Two important factors determine the flow field of a CFD model. These are:

- Geometry definition: The solid body is the geometry around which the wind flows. The geometry chosen for evaluation in this case is a flat plate geometry as seen in Figure 3.1. The model geometry was chosen based on the wind tunnel study by Uslu *et al.* [13]. The dimensions are scaled down in the ratio 1:5 from the model to the real scale. The panel length along the direction of flow is taken as the base dimension, L = 0.2 m. The geometry was found to be acceptable based on prior CFD investigations for low-intensity turbulent flows [9, 69].

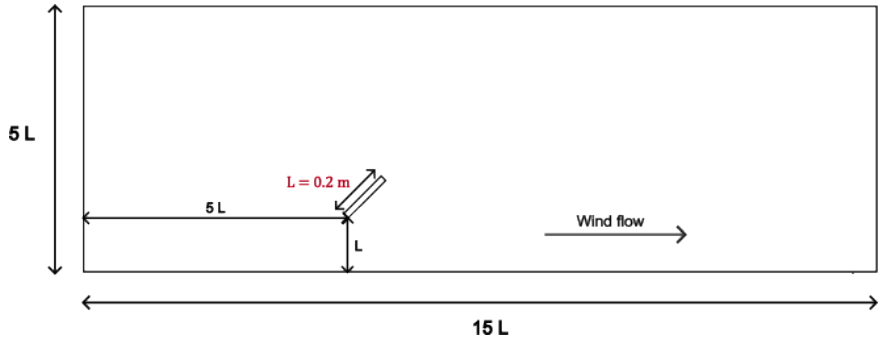


Figure 3.1: Geometric setup for analysis of flow over a 2D flat plate.

- Wind definition: In a real-life scenario, wind loading is a non-stationary phenomenon with wind velocities acting in all directions and constantly shifting. For simplicity, this work considers a stationary wind velocity that is within the atmospheric boundary layer [76]. 2D rectangular domains are used to recreate wind tunnel test setups rather than to mimic real-world conditions. This greatly simplifies a CFD model setup and allows a more structural approach to evaluation. Under the assumption of neutral atmospheric conditions, a logarithmic boundary layer profile is provided as input. The wind speed is described by Equation 3.1 and the velocity profile can be seen in Figure 3.2.

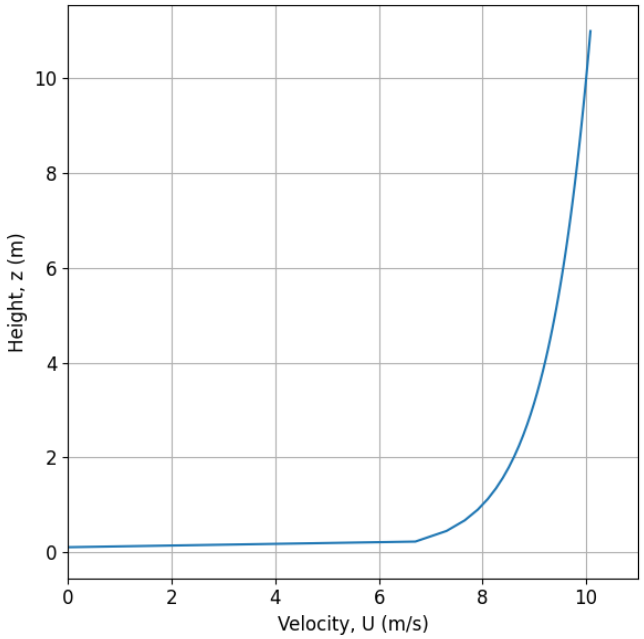


Figure 3.2: Logarthmic velocity profile used for wind flow at heights below 60 m.

$$u(z) = u(H) + u(H) \cdot \left( \frac{\log\left(\frac{z}{H}\right)}{\log\left(\frac{H}{z_0}\right)} \right) \tag{3.1}$$

$u(H)$ : Wind velocity at a known(station) height $H$ (m/s) (usually at 3 or 10 m),
$u(z)$ : Wind velocity at unknown height $z$ (m/s),
$z_0$ : Roughness height of the ground surface (m).

The roughness of the sea is assumed to be between $10^{-4} - 10^{-2}$ m based on the recommended roughness parameter shown in Table 3.1 [12].

| *Terrain Type* | *Roughness parameter, $z_0$ (m)* |
|---|---|
| Open sea without waves | 0.0001 |
| Open sea with waves | 0.0001 – 0.01 |
| Coastal areas with onshore wind | 0.001 – 0.01 |

Table 3.1: Roughness parameters in the sea based on terrain[12].

As part of the wind flow conditions, a parameter called turbulence intensity is also to be provided at the input and output boundaries. Turbulence Intensity(TI) is a measure of the velocity fluctuations happening to the mean velocity profile. TI of 1% is considered as very-low intensity and values greater than 10% are considered as high-intensity turbulence [77]. For wind tunnel experiments, generally turbulence intensities in the range of $1-5\%$ are chosen [16, 9].

Once the flow field is defined, there is a basis for evaluating the body, whether in water or land. The approach taken in this thesis is to first try and simulate wind flow over a flat plate, progress to the geometry of the FPV module, and finally consider flow over water. ANSYS Fluent R2023b is used as the main computational tool. The computational processor used is AMD Ryzen-5 4600H with 8 GB RAM.

### 3.1.2 Mesh definition

The first choice of pre-processing after defining the geometry and flow is the mesh definition. The main choices in the mesh definition are the type of mesh to be used and the size of the elements chosen. Both of these choices affect the accuracy of the solutions and the computational time required by the solver. Thus, it becomes important to define a good mesh for the solver.

The mesh types available are shown in Figure 3.3. Out of these, polyhedral meshes will not be discussed as they are not used in the meshing workflow in defining the model. Triangular/tetrahedral (2D/3D) elements are the default element type in ANSYS Fluent R2023b [77] while quadrilateral/hexahedral elements allow for better discretisation.

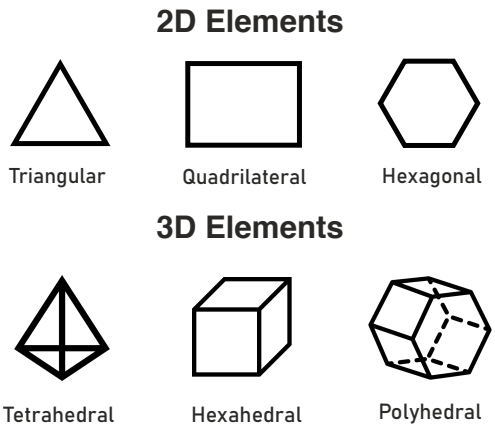


Figure 3.3: Common mesh element types used for CFD analysis

Mesh element size is chosen considering the computational time requirement of the solution and the accuracy of the solution. Generally, lower mesh element sizes provide more accurate solutions but increase the computational time required. The method adopted for the solution is to consider greater refinement of mesh elements in the boundary of the PV panel and a larger mesh size for the surrounding elements.

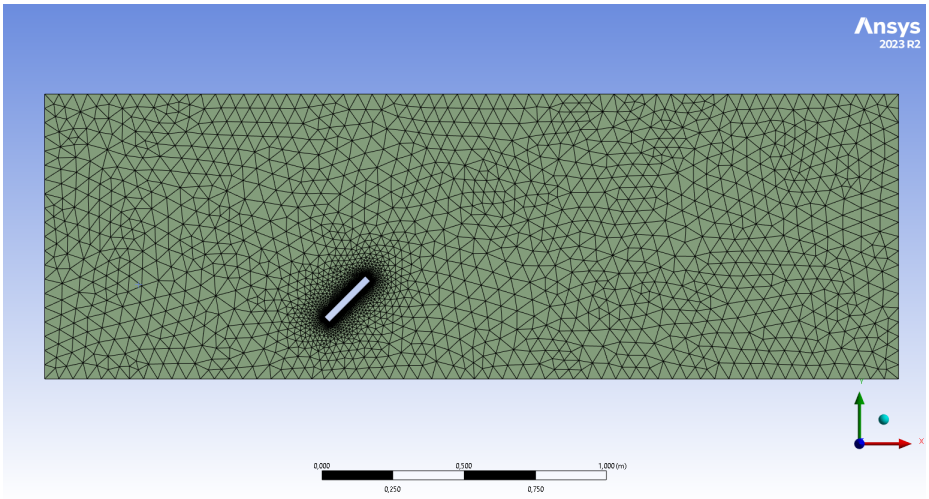


Figure 3.4: Mesh view of a 2D flat plate in a wind tunnel from Ansys Fluent R2023b.

To check the effectiveness of the solver and the model setup, an aerodynamic setup model from the literature is used to provide a base check on the solution accuracy. The 2D setup as shown in Figure 3.4 is used for a 2D mesh study comparing triangular elements and quadrilateral elements. A transient analysis is run for simulating flow over a flat place.

A comparison of the convergence of force in the x-direction is shown in Figure 3.5a. The mesh

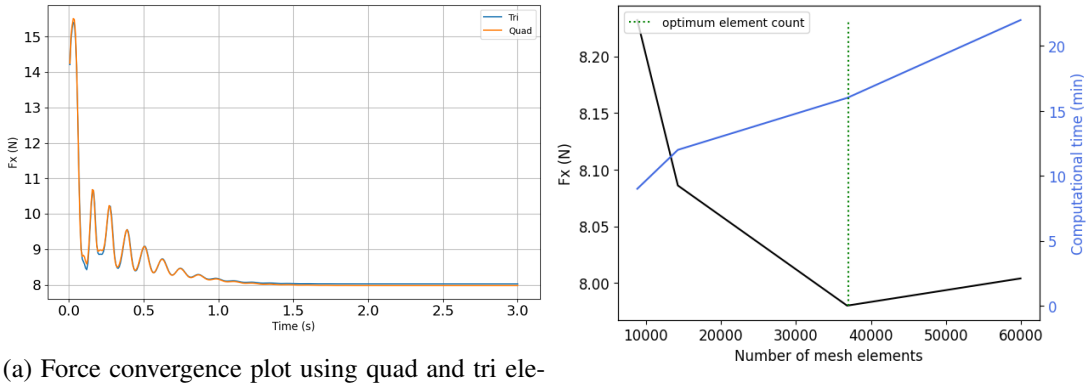


(a) Force convergence plot using quad and tri element mesh types.

(b) Mesh refinement plot for 2D flat plate setup.

Figure 3.5: Mesh study for 2D flow over a flat plate.

with triangular elements was found to take almost twice as long to run than a similarly sized mesh with quadrilateral elements. The results obtained are similar enough that computational cost is much more relevant to the choice of mesh type in this case. This might be different for different solution cases, especially complex geometries where quadrilateral meshes may be difficult.

Going forward with a quadrilateral mesh, Figure 3.5b shows that making a finer mesh improves solution quality but it also increases computational time. A balance of the two is required to gain an accurate solution with affordable computational cost. An increase in mesh element count in this case from 40000 - 60000 only changes the force output by 0.05 N while increasing the computational time by 6-7 minutes. This is an unnecessary computational cost if double-digit accuracy is not required for our application. Therefore an optimum mesh element count in this case would be around 37000.

A 3D setup is also evaluated to compare the performance of 3D mesh elements. The results for the mesh element comparison yield similar results as the 2D case with hexahedral meshes solving faster than tetrahedral meshes with similar results. The results with performance graphs are detailed in Appendix B.

## 3.2 Validation of flat plate model

After conducting 2D and 3D mesh studies, the boundary conditions for flow are applied and the model setup is finalised. The main settings are described in Table 3.2 [13].

Convergence criteria are usually set for residuals of the solution. The residuals represent the magnitude of error in numerical computation for the primary solution parameters of continuity, momentum, and energy. The convergence criterion for this model is defined for the residuals of the solution continuity which is the highest. Acceptable error was defined as 1

| | |
|---|---|
| PV panel | 20 cm x 2.5 cm |
| Analysis type | Transient |
| Wind velocity | 10 m/s at 10 m |
| Wind speed profile | Logarithmic |
| Turbulence Intensity | 5% |
| Flow Model | SST $k-\omega$ turbulence model |
| Solver settings | Coupled P-V |
| Convergence criteria | Continuity residuals $< 10^{-4}$ |

Table 3.2: Single-phase model setup controls.

x $10^{-4}$ of continuity residuals. For transient simulations, convergence based on this criterion was achieved under a simulation time of 7.5 s.

Figure 3.6 shows the general nature of the flow around the panel once the flow field is steady.

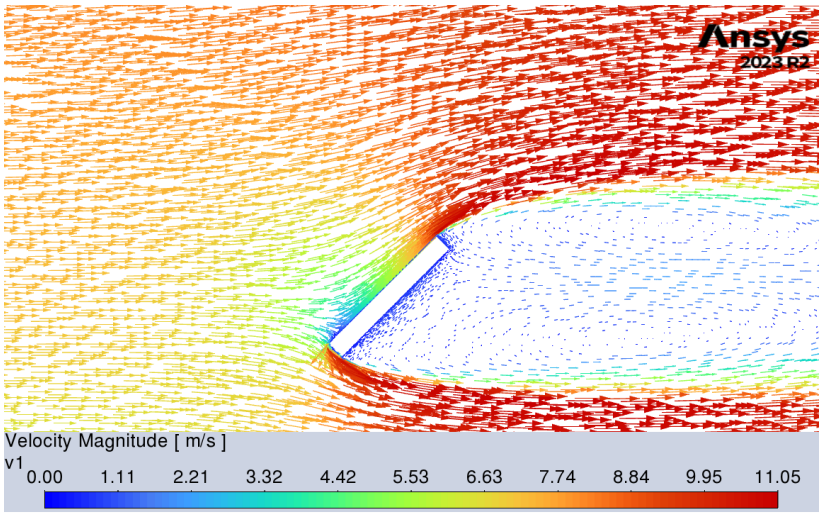


Figure 3.6: Velocity vectors indicating flow over a 2D flat plate setup.

The contours and vectors from the steady-state solution help us understand the direction and magnitude of the forces acting on different areas of the panel and how the flow forms around a flat panel. The drag and lift forces acting on the module inform both the translational and vibrational response of the module to wind loading while the rotational response can be studied by checking the moment acting on the panel. For the PV panel study, the drag and lift coefficients of the modules with increasing horizontal tilt were validated with CFD studies done prior [13, 14, 15, 16].

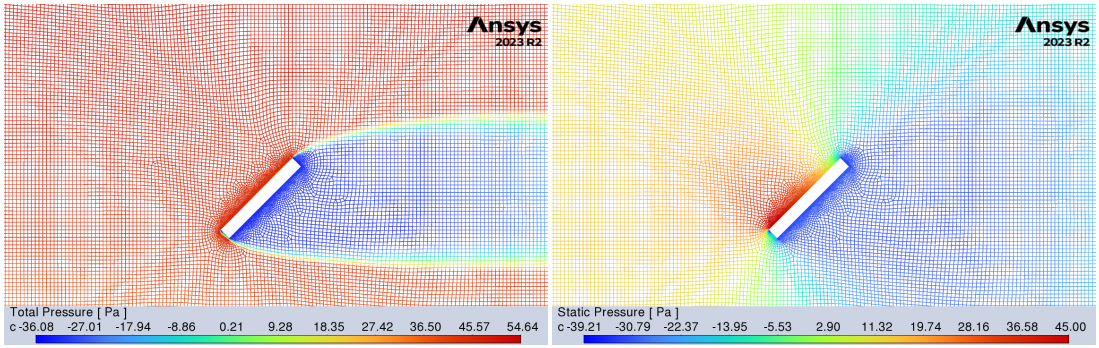


(a) Total pressure contour.

(b) Static pressure contour.

Figure 3.7: Pressure contours for flow over a 2D flat plate.

### 3.2.1 2D model validation

Figures 3.6 and 3.7 show the velocity and pressure behaviour of the flow over the test setup. It is evident from the contours that the flow behavior varies along the length of the plate and this creates a gradient both in case of static pressure and velocity. However, looking at Figure 3.7a, one can observe that the total pressure in front of the flat plate is the same. The value of dynamic pressure at the trailing edge therefore would be around 35 Pa in this case which is more than double the static pressure. This indicates that the dynamic pressure on the trailing edge of the plate is significant and could be subject to fluctuation based on the nature of the flow i.e. laminar, transient, or turbulent. Such fluctuations would greatly impact panel movement and cannot be predicted by static analysis of the model.

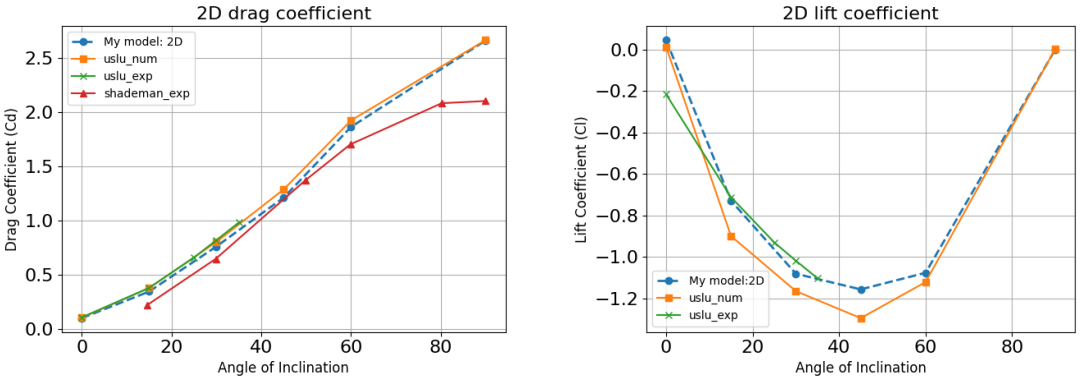


(a) Comparison of obtained drag coefficient with Uslu *et al.* [13] and Shademan *et al.* [16].

(b) Comparison of obtained lift coefficient with Uslu *et al.* [13].

Figure 3.8: Validation study for flow a 2D flat plate.

The validation of the setup was done for varying angles of tilt with the horizontal from 0 - 90°. The drag and lift coefficients obtained from the simulations were compared with those

obtained from literature as seen in Figure 3.8. For the validation, the root mean square error of the measurements was used to provide an estimate of the standard deviation.

The drag coefficient is found to have an accelerated increment till 45°and slow down after that peaking at 90°. Since commercial installations in the Netherlands do not employ solar panels above 45°[78], this means that tilt will significantly affect horizontal forces on the PV module. For the lift coefficient, it has an inverted bell curve with a peak at 45°. This signifies a downward force on the panel which also will have a significant increase in the operational PV tilt angles.

For the drag coefficient, the root mean square error (RMSE) is found to be 0.18. The most significant deviation from the results occurs after 45° tilt. However, considering the general trend of the curves, the measurements do match the behaviour expected. For the lift coefficient, the RMSE is found to be 0.098 and the most significant deviation is observed around the peak at 45°.

### 3.2.2 3D model validation

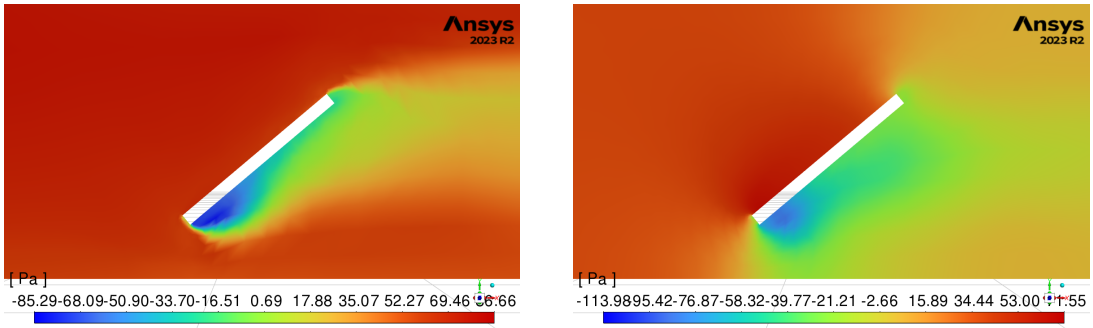


(a) Total pressure contour.

(b) Static pressure contour.

Figure 3.9: Pressure contours for flow over a 3D flat plate.

The 3D setup uses the same input conditions and simulation settings as in Table 3.2. Figure 3.9 shows the pressure contours of the 3D analysis. It is found to be similar to the case of 2D contours.

The validation of this setup is done for drag and lift coefficients for varying angles of tilt as well. Figure 3.9 shows the validation graphs. As seen in Figure 3.10a, there is a proportional increase in the drag with increasing tilt and there is a reasonable match with literature with an RMSE of 0.123 [13]. The lift coefficient also varies in a proportional manner manner as its 2D counterpart (see Figure 3.10b) and a RMSE error of 0.23 is found with the literature. It is also observed that the 2D and 3D models have a good agreement for drag and lift coefficient curves. An overview of the validation is show in Table 3.3.

After performing the validation study and observing the pressure and velocity contours for the setup, the following observations are noted.

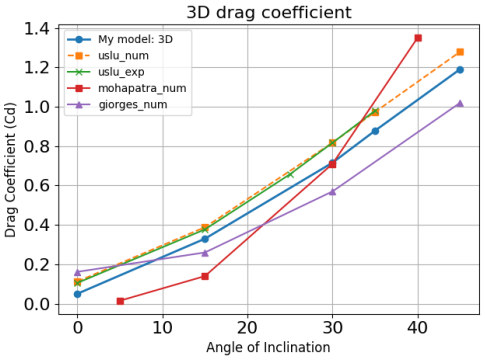


(a) Comparison of obtained drag coefficient with Uslu *et al.* [13], Giorges *et al.* [14] and Mohapatra *et al.* [15].

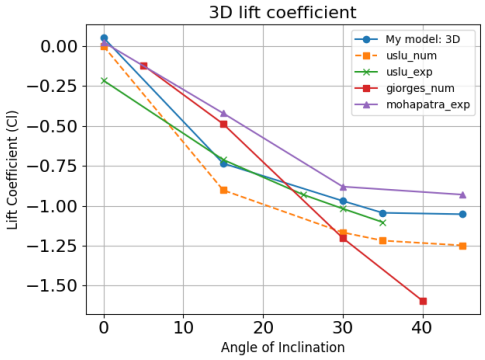


(b) Comparison of obtained lift coefficient with Uslu et al[13], Giorges et al[14] and Mohapatra *et al.* [15].

Figure 3.10: Validation study for flow a 3D flat plate.

| Dimension | 2D | | 3D | |
|---|---|---|---|---|
| Parameter | $C_d$ | $C_l$ | $C_d$ | $C_l$ |
| RMSE Value | $\pm 0.18$ | $\pm 0.098$ | $\pm 0.123$ | $\pm 0.23$ |

Table 3.3: Overview of match with CFD models with literature [13, 14, 15, 16].

- The leading edge of the panel in the direction of flow experiences the highest static pressure, almost twice the static pressure in the trailing edge. The variation of this pressure is also not linear across the plate.

- The trailing edge of the panel experiences fluctuating velocity and pressure fields possibly due to separation induced turbulence (detailed in Appendix A).

- Since both edges of the panel are not uniformly affected by forces, the rotational is thought to be dependent on the nature of the flow more than the magnitude of the forces acting on it.

- Convergence and accuracy of the analysis depends upon the mesh element type and size. Mesh studies help find optimal element size for the study.

- Drag across the panel increases with an increase in tilt and reaches a maximum peak at 90°.

- Lift on the panel acts downward and increases with tilt till 45° and then decreases to zero at 90°.

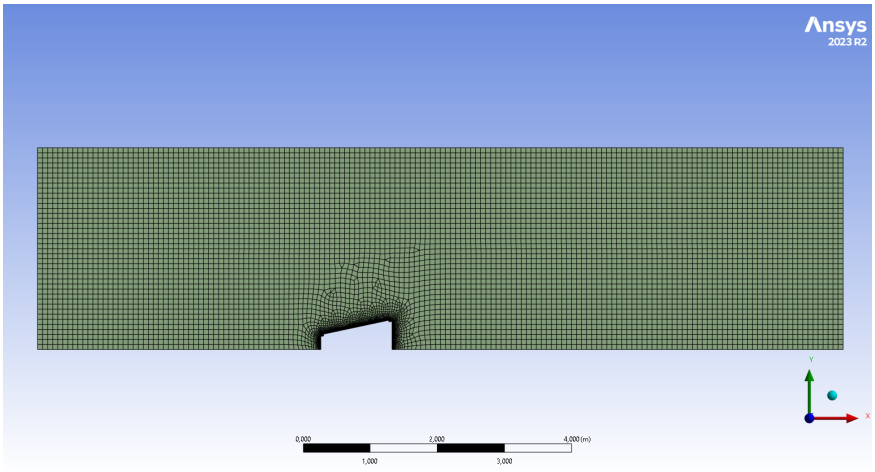


Figure 3.11: 2D Hex mesh of panel attached to floater geometry.

## 3.3 Flat plate with floater geometry

After conducting a transient analysis on a flat plate, a simulation was performed on a geometry with the floater on the PV panel. The chosen setup is similar to individual float-type geometry as defined in Chapter 2. The setup is as shown in Figure 3.11. The intention is again to get an understanding of the wind flow pattern over the structure and identify the zones of maximum force so that it is clear how the module will be affected in floating conditions.

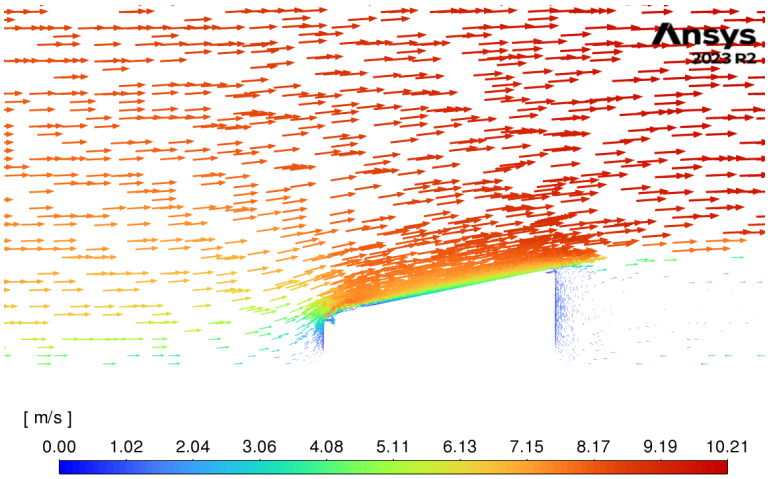


Figure 3.12: Velocity vector of flow around 2D FPV geometry.

The floater geometry is meshed with quadrilateral elements. The boundaries of the geometry are refined and it is placed on the bottom of the tunnel such that there is no airflow below it. The same input conditions and flow settings were used as in the flat plate test validation.

Figure 3.12 shows the flow pattern of the geometry and Figure 3.13 the pressure contours on the FPV module.

The upstream flow experiences the greatest variation in velocity due to the presence of a solid edge perpendicular to its flow direction. This deceleration causes the kinetic energy of the upstream wind to act on the front edge of the module. From the flow contours, it is visible that there are velocity reductions from 5-15 m/s in this region.

For an average velocity of 10 m/s, a maximum static pressure of around 22.6 Pa is experienced on the front face of the module which would amount to a total pressure of 24 Pa. Analytically, the velocity contours indicate a velocity of around 6.26 m/s upwind which if fully converted to pressure on the module would produce an equivalent pressure as shown in Equation 3.2.

$$\frac{1}{2} \cdot \rho \cdot v^2 = 0.5 \times 1.225 \times 6.26^2 = 24 \text{ Pa} \tag{3.2}$$

The largest pressure acting on the floater will be mostly static pressure which does not vary with respect to the flow. It also indicates that due to the direction of application of the force, unrestrained motion will mostly take place as horizontal movement of the module.

A rotational response i.e. a change in tilt angle will however affect the flow. The PV module may be subject to dynamic pressure in this case and it will vary according to turbulence conditions and change as the flow develops. This means that the rotational behaviour of the system cannot be predicted from an initial response or a static analysis. Also, since the PV panel is the most sensitive part of an FPV system, this gives good reason to pursue understanding the response of the system as a transient phenomenon rather than as a static one.

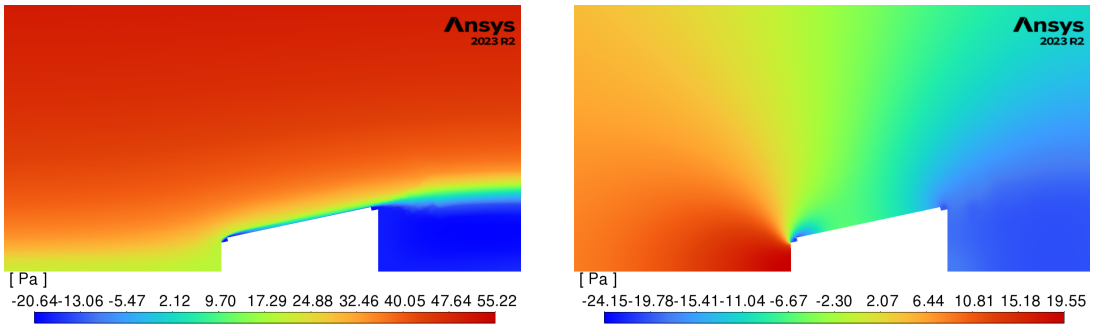


(a) Total pressure contour.

(b) Static pressure contour.

Figure 3.13: Pressure contours for flow over a 2D FPV geometry.

Since there is no gap between the panel and the floater in the 2D geometry we do not see any flow that may cause upward pressure. However, this may also be a cause for concern in a real-life scenario where gaps exist between the floater and the PV panel. The flow visualization also indicates a negative pressure region behind the FPV geometry. This region could affect the properties of the bodies placed downstream of this device.

Validation could not be done for the geometry in the 0° orientation. Since it was found important to study the flow in this orientation the simulation study was conducted and the flow behaviour is noted nevertheless. However, the drag coefficient for flow over the geometry in the reverse orientation (180°) is validated against literature [79]. The results showed a good correlation between the models and the study for the same can be found in Appendix B.

## 3.4 Summary

In this chapter, the types of mesh elements that are available for setting up a wind flow analysis model are discussed. The mesh characteristics, and how to set up a mesh for the problem at hand are also introduced in this section. A flow model was set up in the next section to investigate wind flow over a flat plate. The drag and lift coefficient of the object were evaluated and compared with similar CFD investigations from the literature. This was followed by the addition of a floater geometry on the PV panel and an evaluation of the flow around it. The observation from both the analyses are used to answer the following research questions from Section 1.5

**What is the wind flow behaviour around a PV module?**

From the flat plate analysis, the flow pattern shows the edge of the panel in the direction of the wind is more affected by static pressure, and the flow around the trailing edge is separated and affected more by dynamic pressure forces. The non-uniformity in the forces along the module may cause tilt variations. Hence, the flow behaviour around a module is found to be more important for its rotational response than the forces acting on it. It is also found that there is a significant increase in drag and lift coefficients in the PV panel when the horizontal tilt of the module is increased. Observations are detailed and validated in Section 3.2.

*How do the flow characteristics change with the addition of floater geometry on the panel?*

A flow study in 2D was conducted for an individual floater-type FPV geometry. The flow identified that maximum pressure was experienced on the upwind side of the floater and that the pressure on the PV surface was low. If rotation occurs, the forces acting on the module become difficult to predict and are worth investigating using CFD studies and experimental tests.

The following chapter will discuss the model setup for moving meshes and multiphase flow simulations which are useful for measuring flow behaviour around a floating body.

# 4 Multi-phase Model Setup and Results

The validated aerodynamic models from Chapter 3 are used in this chapter to a multiphase (air-water) model. This model will be used to simulate the tilt response of the FPV module due to wind loading. The chapter begins with a section detailing the necessary settings for model control. This includes two main parts, mesh and solver settings, which will be briefly explained with examples of how they influence the solution. Then, the finalised model will be used to simulate FPV movement under various flow conditions and design variations. Finally, the results will be summarised and used to describe the tilt variation of an FPV module exposed to wind.

## 4.1 Multi-phase modelling setup

After the initial assessment of flow over the geometry is done, a multi-phase model is used to determine how the wind flow will move the geometry. Due to computational constraints, only 2D simulations were possible within the scope of this thesis. This section will be used to briefly introduce the controls and settings that were used to simulate the movement of the module.

A simulation study is performed on the PV with floater setup as from Chapter 3. A fine mesh is generated close to the interface to improve the numerical stability and accuracy of the solution. The setup is as shown in Figure 4.1. Since the preliminary goal of the study is to find out how floating PV yield might be affected by wind loads, the study is limited to the rotational motion of the body. The body is therefore constrained to rotation only about its center of gravity. This can be assumed as a scenario where the body is constrained in translational motion by mooring lines and other FPV modules. This case study, although limited, provides enough information about the device movement and is determined as the best use of existing computational resources to further the study.

To enable the model setup from the single-phase flow analysis to solve a multi-phase flow problem, several model settings needed to be optimised for computational efficiency. The most important of these settings were chosen based on preliminary simulation studies done

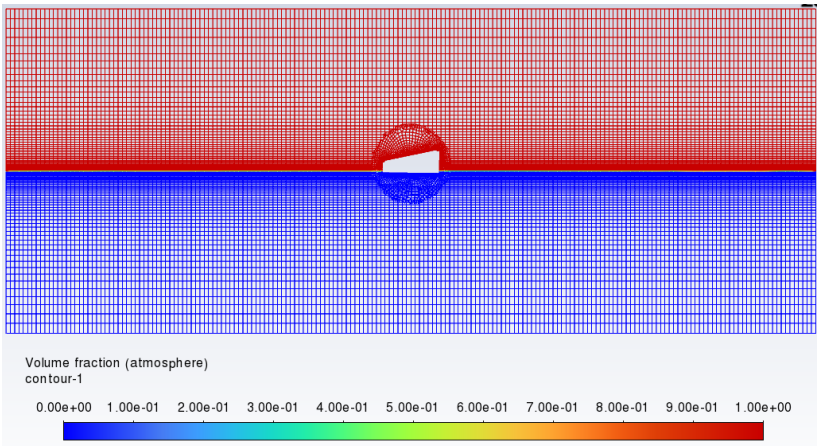


Figure 4.1: Phase contour of the multiphase model with the 2D FPV on the water surface.

on a multi-phase test model based on the single-phase flow problem (settings from Table 3.2). The most important model settings that were modified will be discussed in this section. These are:

1. Solution controls: The computational settings that allow the software to solve the flow problem and yield a numerically accurate solution that is also computationally affordable.

2. Mesh movements: The dynamic mesh settings which allow rigid body motion. There are different possible options for describing body movement in ANSYS and different meshing techniques that can be used to accommodate such movement during the simulation.

### 4.1.1 Solution control

There are various aspects of solution control to ensure an accurate and computationally efficient simulation. Since the methodology of developing a model is important to this work, it is necessary to discuss these settings in the context of the work done. Solution control in this sense involves:

1. Solver choice: Choosing an appropriate solver for the flow problem and a good spatial discretization scheme to aid the solution convergence.

2. Time step control: Determining how fast the solution should compute and how the time advancement of the solution is computationally made stable.

### Solver choice

Selecting a good solver is essential to how the solution progresses. CFD analysis is done by solving the Navier-Stokes equations. Common commercial CFD software use averaged flow models like Reynolds Averaged Navier Stokes (RANS) equations for steady and unsteady flows. This has a wide range of applicability from single-phase flow over airfoils to multi-phase reactor flow involving dispersed phases. The continuity equation (Equation 4.1) and the Navier Stokes Equation (Equation 4.2) are the bases of computing the flow solutions of all these problems.

$$\frac{\partial u_i}{\partial x_i} = 0 \tag{4.1}$$

$$\rho \frac{\partial u_i}{\partial t} + \rho u_j \frac{\partial u_i}{\partial x_j} = -\frac{\partial p}{\partial x_i} + \frac{\partial t_{ji}}{\partial x_j} \tag{4.2}$$

From Equation 4.2, it is visible that four main terms define the flow. These are the velocity ($u$), density ($\rho$), pressure ($p$), and time ($t$). The solver uses existing information from the flow field and solves the differential equation using numerical methods. These methods are varied and should be chosen depending on the solution desired. For a multi-phase solution, the solver settings for all the terms except density will be important [77].

One of the first choices to be made is to define the turbulence as an averaged and stationary quantity to create a RANS equation. For the simulation study at hand, this is done by choosing a 2-equation Shear Stress Transport (SST) $k-\omega$ turbulence model [80]. The $k-\omega$ model comprises two components, the turbulence kinetic energy (k) and the specific dissipation rate for turbulence ($\omega$) which help implement the computation. The model is particularly useful to compute near-surface and free-flow effects. This allows it to work well for analyzing wind loading on floating devices where different scales of flow analysis are required. For multi-phase solutions the Volume of Fluid (VoF) model is used in tandem with this solver and interfacial diffusion is turned on to model a sharp interface [77].

After choosing the primary solution model, then a choice is made for the numerical solver. Of the solvers provided in ANSYS Fluent 2023b, SIMPLE and SIMPLEC solvers are the fastest solvers but the toughest to converge. From simulation studies on the multiphase test model and the box mode(see Appendix C), using the SIMPLE solver is found to be faster than the other solvers available: 40% faster than the PISO model and 75% faster than the coupled solver. However, due to the quick solve, it is difficult to achieve convergence with this solver and it generally requires smaller time steps for solution convergence. In many cases, the small time step increases the computational time of the SIMPLE solver more than the PISO or coupled solvers which can handle greater time steps. The time step necessary for the convergence of the SIMPLE solver running the multi-phase test simulation was in the order of 10-100 $\mu s$, the PISO solver was chosen as a more affordable option which allowed for time steps of 200-500 $\mu s$ to be used in the model.

#### Time step control

Once the spatial solver settings are fixed, solvers also require information on how to adapt the solution to time variation. Lower time steps allow the solution enough time for convergence and an accurate solution, although it requires longer computational time. If the time step is very high, the solution obtained might no longer be numerically stable or accurate despite a quick run time. Hence, variation in time step is also a setting that needs close monitoring.

Generally, there are two types of solver methods for time-stepping, these are explicit and implicit methods. Implicit methods adapt step size automatically based on the previous solution and initial guesses. This can be very convenient and the only option for some solvers such as the coupled solver for multi-phase flows. Explicit solvers in CFD on the other hand are more controllable and customisable through a non-dimensional variable called the Courant number [77]. The Courant number is a measure of how fast the flow proceeds through a single mesh element and can be estimated by using Equation 4.3.

$$C = \sum_i \frac{U_i \cdot \Delta t}{\Delta h_i} \tag{4.3}$$

Here, $U_i$ refers to the velocity of flow through an element i, $\Delta t$ is the timestep of the simulation and $\Delta h_i$ is the height of the mesh element.

Generally, it is good practice to keep the Courant number under 1 for an accurate and converged solution [81]. Based on the solver choice of PISO, time step limits are around 200-1000 $\mu$ s, and the mesh size chosen is 1-8 mm (results in Appendix C). Courant numbers in the range of 0.1 - 1 are calculated as viable for the simulation study.

### 4.1.2 Mesh Movement

The movement of the object during the simulation causes the flow field to deform which disrupts the calculation. To repair the deformed mesh and compute the solution for a moving object, two possible options are covered in this section. These are dynamic meshes and overset meshes. Both of these mesh movement types can be used with the six DOF solver [77] which prescribes rigid body motion to an object using its mass, center of gravity, and moment of inertia values. Case studies have been performed with the multiphase test model for both these types of meshing types to find out their use case and they will be described below.

#### Dynamic Meshing

Dynamic meshing in this thesis refers to the default form of meshing available in ANSYS. When an object moves in the flow field, it stretches the mesh elements next to it and makes them highly skewed. After a certain point of skewness, the stretched mesh elements surrounding the moving object create new mesh elements based on the skewness requirements

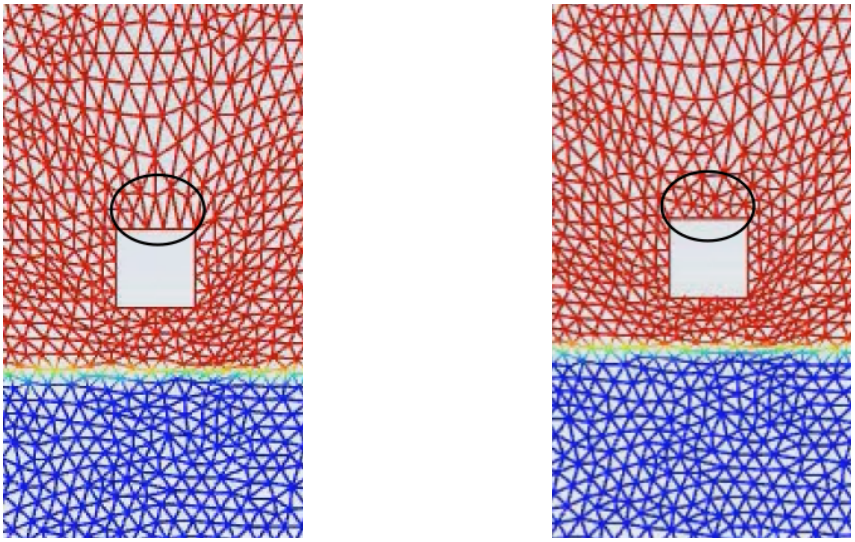

(a) Mesh elements stretched due to movement.

(b) Re-meshing of stretched elements.

Figure 4.2: Zoomed in picture of a 2D box falling in water affecting the mesh around it.

provided. As an example, pictures of the mesh stretching and re-meshing for a box falling into water are shown in Figure 4.2

This type of meshing is found to be possible for the given geometry only using triangular elements. This increases the computational load of the setup drastically and creates an issue with numerical stability as well. While simulating the 1D rotation of a 2D box in water, the dynamic meshing required 7-8 hours to simulate 1s of movement. This high computational requirement also does not even guarantee an accurate and stable solution (further details in Appendix C). This computational time and numerical instability further increased when simulating the FPV geometry which has smaller edges and an angular shape. Thus, it was necessary to look for an alternative meshing option to simulate the movement of the FPV module.

### Overset Mesh

Overset meshing is a meshing technique that allows the user to incorporate moving bodies in a CFD setup that has large amplitude oscillations. An overset mesh is a component mesh with the moving object placed on top of a background mesh with the fluid. The overset mesh used in the setup is shown in Figure 4.3a.

The overset mesh moves as a whole and does not deform which allows mesh properties near the FPV body to be more consistent. The interface with the background mesh is what is being reconstructed with the movement. As long as there is no significant overlap between the mesh faces and node elements, this meshing technique yields a much more stable and computationally efficient solution for the wind loading application. Simulation tests for the multiphase test model yield an 80% reduction in computational time for the same solution

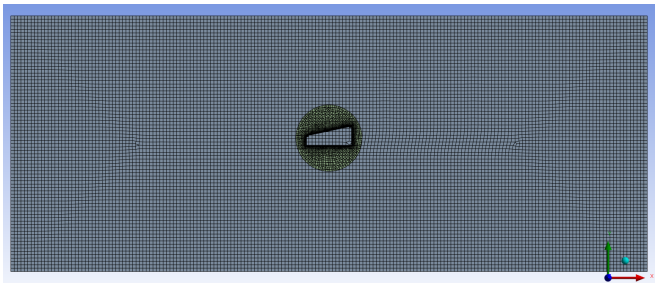

(a) Fluid mesh in the background and FPV component mesh in the center.

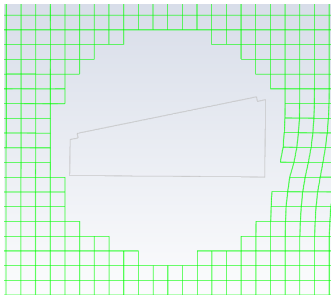

(b) Zoomed in view of the cutout of the overset mesh in the background mesh.

Figure 4.3: Overset mesh of an 2D FPV panel.

accuracy as dynamic meshing. Therefore, overset meshing is chosen for the multiphase model setup.

## 4.2 Case Studies

As the most important parts of the setup have been discussed in the previous sections, all of this information is used to set up the multi-phase model as shown in Table 4.1.

| | |
|---|---|
| Flow Models | Multiphase VoF model<br>SST $k-\omega$ turbulence model |
| Solver settings | PISO solver |
| Discretisation | Second order upwind scheme for momentum and turbulence variables<br>Compressive scheme for volume fraction<br>PRESTO! for pressure |
| Time-step control | Explicit Scheme<br>Courant number $0.1-1$ |
| Mesh type | Overset mesh |
| Fluid Boundary | 15m x 6m |
| Inertial properties | m = $32kg$ $I_{zz}$ = $2.9614kg.m^2$ |
| Initialisation | Hybrid |
| Convergence criteria | Residuals of continuity and turbulence $< 1e-5$ |

Table 4.1: Multi-phase model setup controls.

The model is used to investigate four different parameters: two flow parameters and two geometric parameters. The flow parameters are wind velocity in the x direction and direction of flow, while the geometric parameters are the horizontal tilt variation of the PV panel and the floater height. The results obtained for each will be detailed in the following sections.

### 4.2.1 Movement variation with velocity

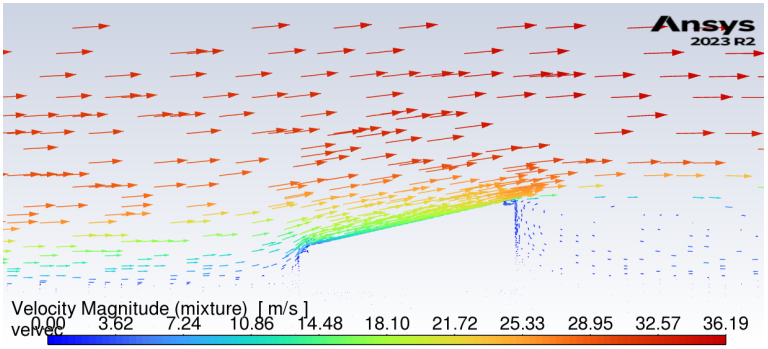


Figure 4.4: Velocity vectors of flow at 40 m/s.

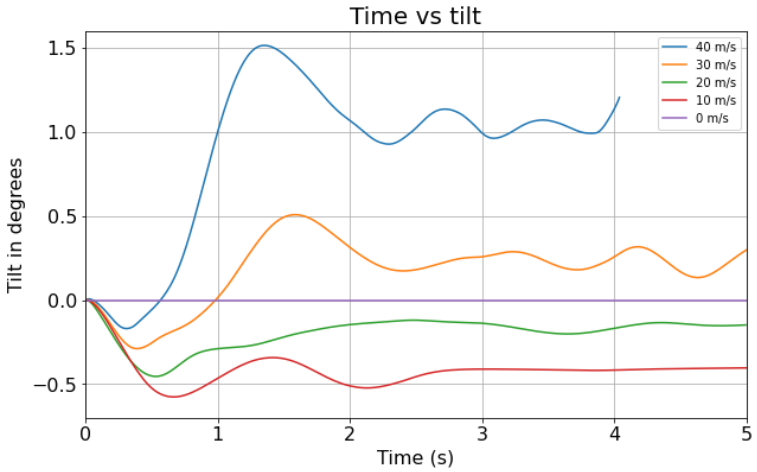


Figure 4.5: Rotational movement of the FPV under different wind velocities.

The body was subject to velocities as a logarithmic profile in the x-direction. The standard wind velocities were chosen at a height, of H = 10 m. The simulated velocities are 0, 10, 20, 30, and 40 m/s which range from still water conditions to rough sea wind conditions. The tilt behaviour was simulated for a period of 5 s and is shown in Figure 4.5.

From Figure 4.5, some notable observations are:

- Maximum tilt variation even for the highest wind velocity of 40 m/s is within 2°.

- Maximum tilt (positive or negative) occurs in the first peak and then it stagnates.
- The dynamic response of the device to wind load becomes increasingly non-linear with higher velocities.
- Change in rotational direction from clockwise to anticlockwise for increased wind velocity.
- A dip is observed in the tilt before the velocity profile reaches the geometry.
- The dip reduces with an increase in velocity.

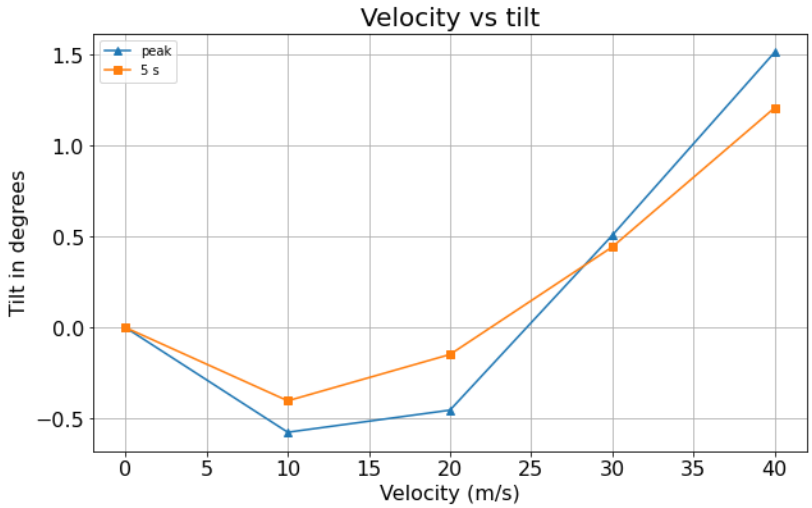


Figure 4.6: Trend plot of rotational peak and 5 s tilt values under different velocities.

At low velocities, the tilt values are negative, signifying device rotation in the clockwise direction. The trend followed for the peak values of tilt and the tilt at the end of the simulation is plotted against velocity variation and can be seen in Figure 4.6. The trend shows a change in tilt direction that happens around 25 m/s which causes higher velocity values to cause rotation in the anti-clockwise direction.

From the pressure and velocity contours, it is assumed that the change in rotational direction may be due to differences in flow behaviour at different velocities. In the 10 m/s setup, the pressure contours in Figure 4.7a clearly show a separation occurring at the leading edge of the panel which causes the flow to bypass most of the PV module. This separation causes the module to experience low pressure at the leading edge and a positive pressure gradient towards the trailing edge which leads to clockwise rotation.

In contrast, the flow over the module at 40 m/s as in Figure 4.7b indicates a much smaller flow separation over the leading edge of the module. This would cause greater pressure at the leading edge of the module causing an anti-clockwise tilt at higher velocities. The flow separation happening at the leading edge is therefore thought to affect the directional tilt of

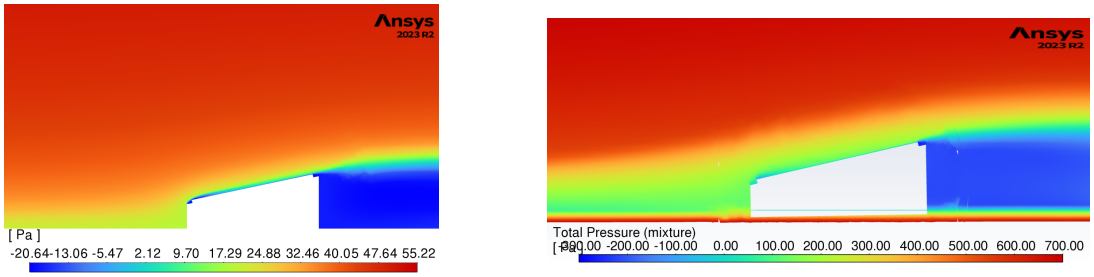


(a) Total pressure contour at 10 m/s.

(b) Total pressure contour at 40m/s.

Figure 4.7: Pressure contours of panels affected by different wind velocities.

the module and further investigations need to be conducted to determine how this behaviour changes.

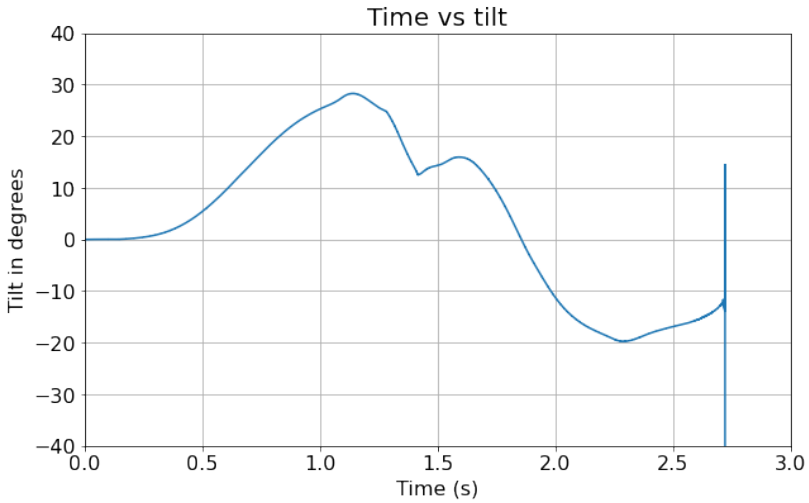


Figure 4.8: Extreme computational case of tilt variation of FPV at 100 m/s.

Due to the low tilt variation observed for the given velocities, a velocity of 100 m/s was provided to observe a computational maximum. This solution turned out to be numerically unstable under the conditions of the setup. However, the tilt variation in the simulated period of 2.7 s is shown in Figure 4.8. A maximum numerically stable peak of 28° is observed at 1.1 s after which the solution becomes unstable in the period between 2.5 - 3 s. This study indicates that the movement of the FPV module is not restricted due to the model setup. It is also interesting to note that in this case there is no initial dip observed.

### 4.2.2 Movement variation with wind flow direction

To see how the module moves when the wind flows from the other direction, the orientation of the module is changed and the simulation study is done for 40 m/s velocity. The observed

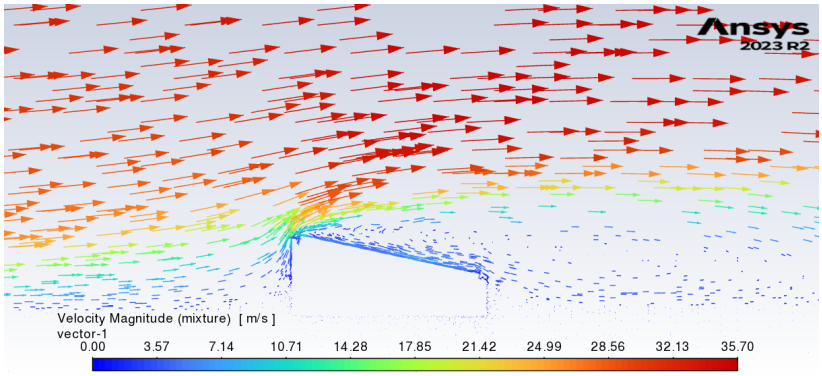


Figure 4.9: Velocity vectors of flow around the revered orientation FPV at 40 m/s.

flow for the reversed orientation is shown in Figure 4.9.

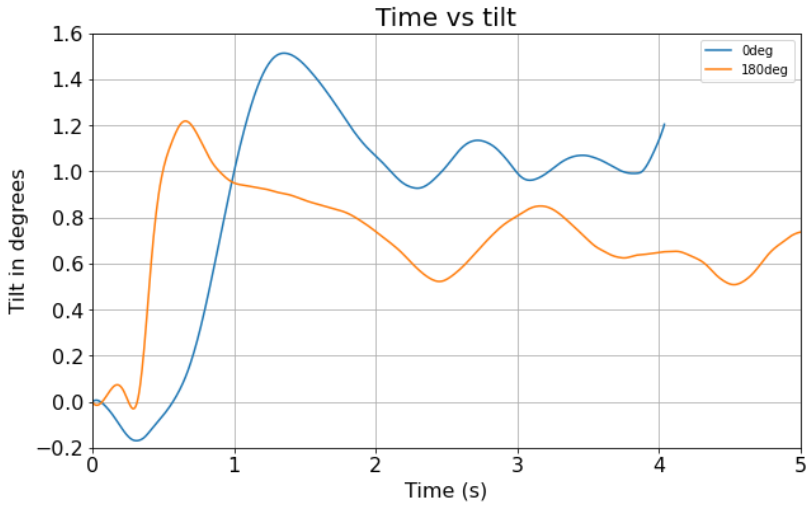


Figure 4.10: Rotational movement recorded for change in orientation at 40 m/s (0° is normal orientation and 180° is reversed).

The results for the rotational response of the module compared to the normal orientation variation are shown in Figure 4.10. The magnitude of the rotational response is found to be lower for the reversed orientation. The dynamic response of the module is also found to be different from its counterpart. The rotational peaks and dips are found to be of higher amplitude and lower frequency.

To check the effect of flow on the rotational response of the device, the total pressure contour is also analyzed. Figure 4.11 shows the variation in total flow pressure around the module. The flow is seen to experience a high degree of separation-induced turbulence at the corner of the module which causes the formation of a low pressure zone on the entire module except for the front edge. This means that the high-pressure regions are the front edge and the submerged

part of the floater. Since the front edge has a uniform pressure distribution and the center of rotation is above the midpoint, this may cause an anticlockwise tilt.

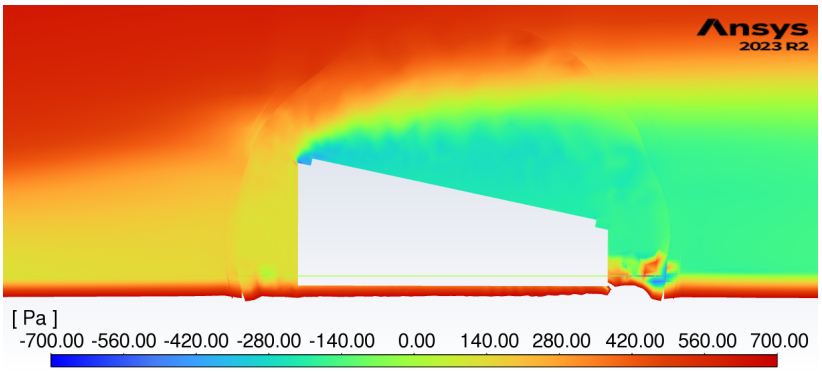


Figure 4.11: Pressure contour of the FPV module in a reversed orientation.

To investigate if there is any change in forces acting on the module in the reverse orientation as opposed to the normal orientation. The forces acting on the module are also plotted for the length of the simulation. The comparison is seen in the Figure 4.12.

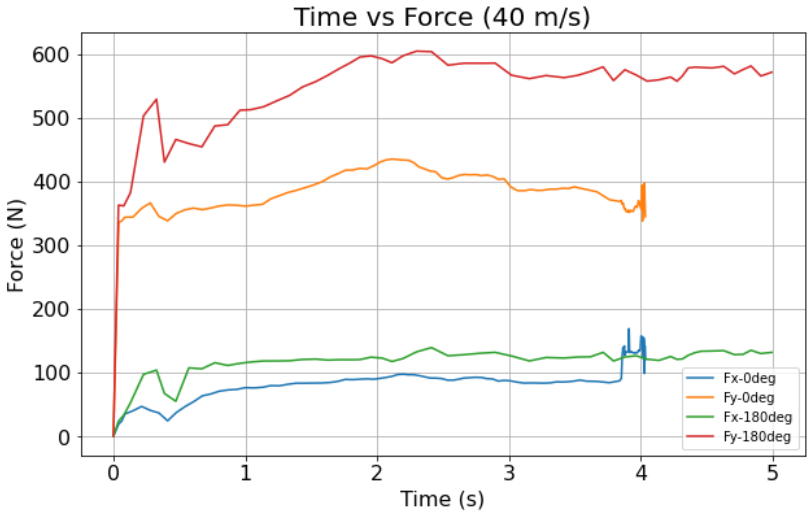


Figure 4.12: Force comparison for normal (0°) and reverse (180°) orientation for the simulation at 40 m/s.

It is seen that there is a much higher force acting on the FPV module both in the horizontal and vertical direction even though a lower tilt is observed. Compared to the normal orientation, the vertical force acting on the object is found to increase much higher than the horizontal force which may cause translational motion in the y-direction if unrestrained. This also indicates that the amount of force acting on the body need not correlate to the rotational tilt response.

### 4.2.3 Movement variation due to tilt of module

To investigate the effect of geometry change, the FPV movement was simulated for different values of horizontal tilt. The chosen values of tilt were 0°, 12°, 24°, 30° and 36°. Higher angles are not chosen as the optimum tilt angle in the Netherlands is found to be under 36° [78].

| Design tilt of FPV (degrees) | Mass of FPV (kg) | Center of Gravity | Moment of Inertia ($kg.m^2$) |
|---|---|---|---|
| 0 | 28.63 | (0, 0.180) | 2.50 |
| 12 | 32.00 | (0.549, 0.273) | 2.96 |
| 24 | 36.48 | (0.566, 0.370) | 3.77 |
| 30 | 39.27 | (0.575, 0.418) | 4.40 |
| 36 | 42.63 | (0.585, 0.482) | 5.32 |

Table 4.2: Changes in geometric parameters of the module with tilt.

When changing the tilt angle of the device, to make the geometry consistent with the other studies, the smaller front edge of the floater is kept at a constant length and the angle of the upper edge of the floater along with the PV on it is changed. This change would proportionally cause a shift in the centre of gravity of the module and the mass moment of inertia of the system. Since the volume of the system also changes, a proportional change in the mass of the floater is also taken into account for the calculations. These changes are noted in Table 4.2 (Notes: The centre of gravity is measured from the left corner of the module).

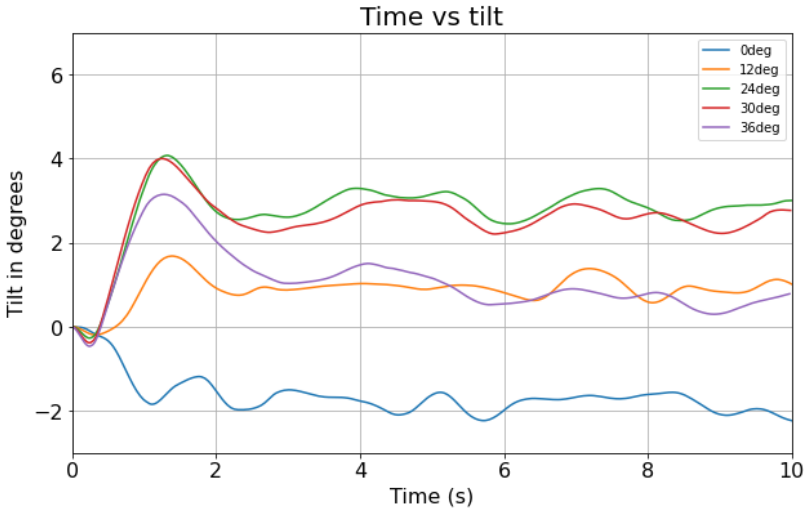


Figure 4.13: Rotational movement with variation in the horizontal tilt of FPV geometry.

While setting up the simulation study, it was found that increasing tilt made it difficult to complete the simulation. The solution was found to diverge at the 3-4 s mark based on the

particular angle. A fixed time step of 0.001 s and a relaxation in the residual convergence criteria from 1e-5 to 1e-3 yielded less variation in the forces acting on the body. These settings were also computationally less time-consuming and hence chosen for the simulation study.

Figure 4.13 shows the variation due to tilt conducted using this study. The pattern of results shown makes it difficult to understand a pattern on its own. To get a better understanding of the response patterns, first, the pressure distribution of the two extreme tilt variations is compared to understand the effect of flow behaviour on change in the rotational direction.

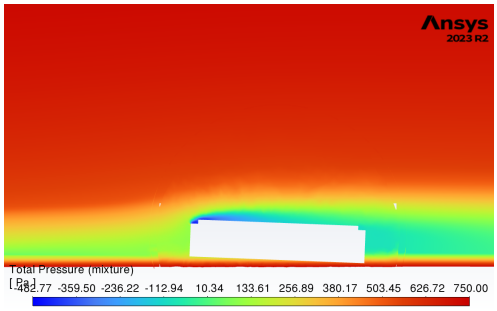


(a) Panel with 0° tilt.

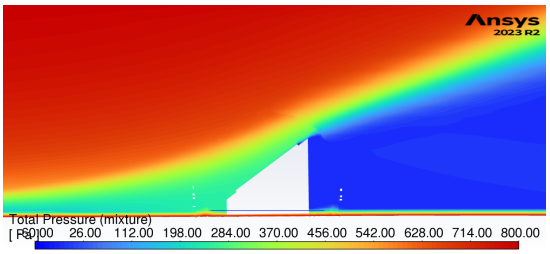


(b) Panel with 36° tilt.

Figure 4.14: Pressure contours of panels with different tilt angles.

Figures 4.14a and 4.14b represent the pressure contours of the two extremes of this parametric study. It is seen that flow separation occurs at the leading edge of the 0° panel and creates a low-pressure region. In the trailing edge, however, the pressure is higher which indicates the clockwise movement of the module. When looking at the 36° tilt, module, there seems to be no flow separation at the leading edge, and upon the inspection of nodal probes, it is found that the pressure on the leading edge of the module is greater than the trailing edge and this induces a movement in the anticlockwise direction.

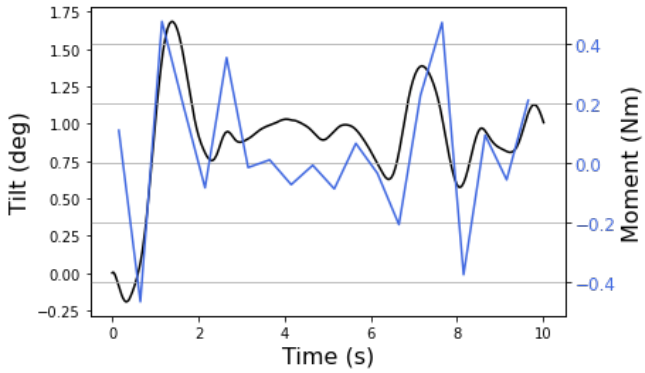


Figure 4.15: Moment forces acting on the FPV with 12° tilt along with its rotational response.

The moment on a body represents the net rotational force acting about a center. The moment forces acting on the body can be compared with each other to understand the dynamic response

behaviour. Figure 4.15 shows that the peaks of the net moment variation of the body about its center of gravity is aligned with the tilt variation. The match between the two curves shows that moment peaks can be a good indicator of the rotational movement of the module.

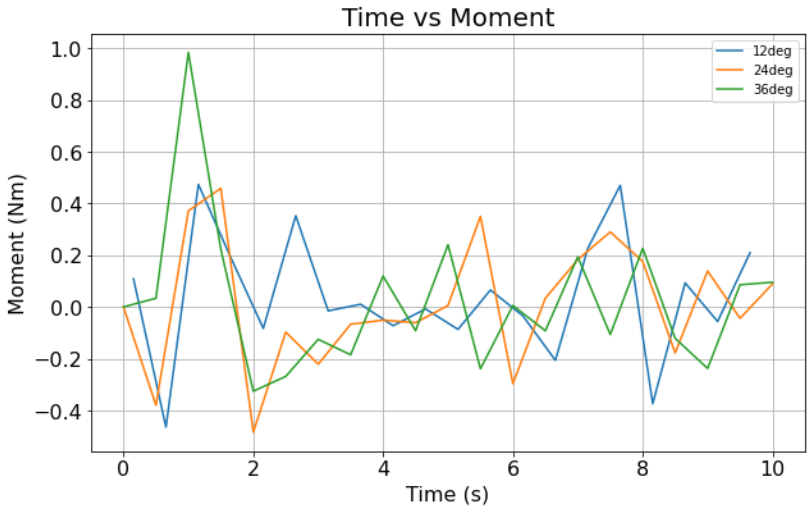


Figure 4.16: Moment variation of the 12°, 24° and 36° test cases for a period of 10 s.

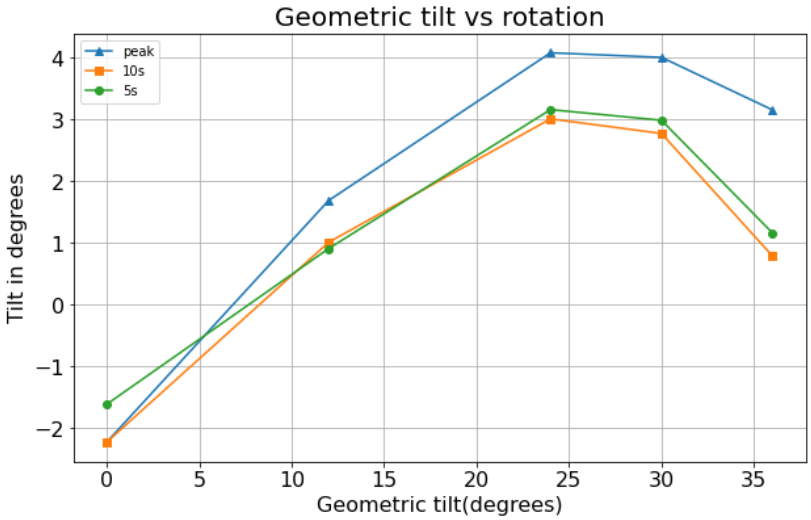


Figure 4.17: Trend plot of rotational peak, 5 s and 10 s tilt values under different module tilt.

Figure 4.16 shows the inverted moment variation of three study cases, 12°, 24°, and 36° tilt. It is seen that the moment variations for the different design tilts, the overall range is similar ranging mostly from -0.4 to 0.4 Nm. However, for the moment peaks, it is observed that the highest tilt geometry produces a predominant primary peak followed by several peaks which are much smaller in comparison. The 12° and 24°tilt modules have milder primary peaks and significant peaking following that at 5-8 s with the 12° module having a secondary peak

almost as high as the primary.

The general trend of the rotational movement for different design tilts is visible in Figure 4.17. It is observed that there is an increase in peak rotational tilt with the increase in horizontal tilt angle until 24° and then a dip is observed. This is the same case for the 5 s and 10 s tilt response trends as well. The 5 s and 10 s responses are also very similar rotational responses and indicate a convergence which could tend to an equilibrium response. The trend indicates a different flow behavior at increasing tilt angles which causes the net rotational movement of the body to be less prominent.

### 4.2.4 Movement due to variation in floater height

The simulation study for 24° device tilt yielded a very high result and it was decided to investigate if the floater height in this module would have a significant effect on the response of the device. Therefore a simulation study was conducted with a modified floater height of 20 cm more than the normal-sized floater. Figure 4.18 shows that the device with the modified floater height significantly increases overall tilt, which was not observed due to a corresponding change in the device tilt.

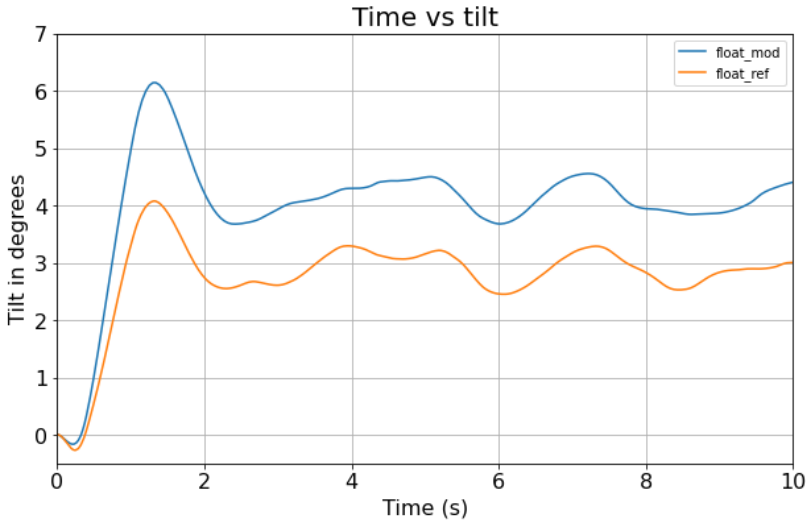


Figure 4.18: Rotational movement in the numerical model with a reference floater height ($float_{ref}$) and one that is 20 cm higher ($float_{mod}$).

Shifting the center of rotation of the device upward and providing more surface area on the leading edge of the floater might have provided a greater moment on the device. The recorded moment of the bigger floater is on average greater than five times the equivalent moment for the normal-sized float. The response plot for both simulations however follows the same trend indicating that the transient response behavior is unaffected by changes in floater height.

## 4.3 Summary

In this chapter, the setup of the multi-phase model is described with emphasis on what the most important settings are for evaluation. This was followed by a parametric study on a 2D setup to find the rotational movement of the device in response to wind. The following research questions from Section 1.5 are answered with the help of this chapter.

**What is the tilt variation of an FPV module exposed to wind?**

From the simulations conducted, it is found that a steady stream of wind causes a rotational movement of the device that experiences a rotational peak within the first 2 seconds and then is subjected to hydrodynamic damping. The damping is found to be non-linear at velocities higher than 10 m/s and no equilibrium point is observed within the time frame of the simulation for these test cases. The highest rotational response of 4.07° (anticlockwise) was observed for a design tilt of 24° and a wind velocity of 40 m/s. The lowest response of 0.1° (clockwise) was recorded for a design tilt of 12° and wind velocity of 20 m/s. The direction of rotation is determined by both the wind velocity and the design tilt of the FPV device and requires a detailed investigation.

*What are the most important CFD model settings that are critical to this problem?*

The spatial solver settings, the time step settings, and the mesh movement are found to be the most critical parameters in the evaluation of the movement in a 2D multi-phase model setup. The spatial solver settings are found to mostly affect the computational time required while the time-step settings and the mesh movement type are also found to affect the ability of the software to compute an accurate and stable solution.

*What is the tilt variation of the module in response to different geometric and flow parameters?*

Four different parametric studies were done on the multi-phase model to determine the rotational response to different flow conditions and differences in the geometry. The parameters used for this study are wind velocity, wind direction, panel tilt, and height of the module. The wind velocity of the module and the initial tilt of the module are found to cause a proportional increase in the anticlockwise response of the device. Clockwise rotation is found more likely to occur at lower design tilt and wind velocities. It is found that the wind rotates the FPV more when the shorter end of the floater is facing the flow. It is also noted that an increase in height of the shorter side by 20 cm leads to more than 2° additional rotational movement signifying this part of the geometry to be critical to wind loading.

# 5 Discussion

The discussion chapter will analyse the results from Chapters 3 and 4, understand the general trends observed, and discuss the suitability of the current methodology for assessing FPV performance. The first section will be a discussion of the numerical results obtained from CFD analysis. The force variation in the x and y direction is compared with the drag and lift variations which are validated in Chapter 3. Then the results from Chapter 4 will be summarised and their significance in predicting a dynamic response will be discussed. The second section will use an analytical model to check if the rotational response of the device is reasonably accurate and then discuss the possibility of numerical errors in the simulation. The final section will be used to determine the advantages of using CFD as a performance assessment tool and if it justifies the computational effort required. This will be used to answer the final research question on the benefit of using the methodology in this thesis to assess FPV performance.

## 5.1 Discussion of Results

Four separate parametric analyses are done on the individual floater PV system using CFD. The studies evaluate tilt angle variations due to velocity variation, wind direction, height of the floater, and the tilt angle of the setup. This section will be used to summarise the main results from the simulation, discuss the trends observed, and analyse how they might be useful to describe the motion of the PV panel with the floater.

### 5.1.1 Wind load variation

In Chapter 3, transient flow is evaluated over a stationary PV panel. The drag and lift coefficients of the module were evaluated for a wind speed of 10 m/s. It was identified that the drag coefficient of the PV panel increased in response to an increase in tilt angle while the lift coefficient of the module had a negative gradient.

Figure 5.1 shows the variation of the peak forces and 10 s forces in response to variation in design tilt for the multi-phase model. The wind speed used is 40 m/s and the 10 s force is taken as the force acting on the module at the end of the simulation period of 10 s.

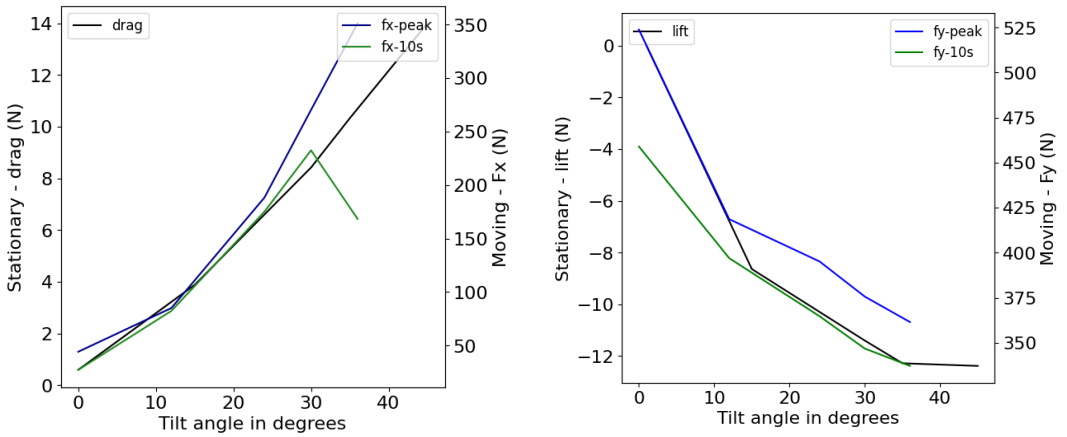


(a) Drag forces plotted against $F_x$.

(b) Lift forces plotted against $F_y$.

Figure 5.1: Variation of peak (blue) and 10 s forces (green) with object tilt in the multi-phase model compared with drag and lift results from the validated 2D PV panel model.

The peak horizontal ($F_x - peak$) and vertical forces ($F_y - peak$) are found to follow a similar pattern as their stationary counterparts when the tilt angles are varied. The peak horizontal and vertical forces occur when the input wind profile first impinges on the device. This would be similar to stationary loading as the body has yet to change its orientation to the wind flow. Therefore, the similarity in the force variation indicates a positive correlation with the validated stationary device response. The equilibrium forces in the x and y directions exhibit a non-uniform variation pattern across different tilt angles. As illustrated in Figure 5.1a, the tilt angle of 30° represents a numerical inflection point for $f_x$ values. Notably, this inflection is not reflected in the corresponding $f_y$ values, suggesting a variation in flow behaviour. This phenomenon aligns with the observed changes in rotational response and moment variation at the same angle, as discussed in Chapter 4. The exclusive impact on x-directional forces suggests that horizontal forces may exert a more pronounced influence on the module's rotational dynamics.

It is also interesting to compare the peak forces and 10 s forces which are extremely close to each other as in 12° tilt which indicates a certain consistency in the force acting on the body with time. In contrast, there is a relatively bigger dip in the 10 s forces from the peak forces for 24° which indicates greater variation in the forces acting on the device. This difference could give insight into the difference in the flow behaviour acting on the device which affects the wind loading on the device.

### 5.1.2 Dynamic response behaviour

A study was done on the variation in tilt due to wind velocities ranging from 0 to 40 m/s, approximating conditions from still water to rough seas. As anticipated, the system exhibited increasingly non-linear response behavior with increasing flow velocities. With increasing

Reynolds Number of the flow, one would expect the same input conditions to produce progressively turbulent behavior. The turbulent flow impacting the leading edge of the body causes the non-linear movement which would require a longer period to stabilize, rendering precise prediction of module tilt more challenging. The simulation results corroborated this hypothesis.

Interestingly, the studies revealed that increased wind speeds also induced a change in rotational direction. An increase in the anticlockwise rotation was observed for wind velocities greater than 15 m/s. This unexpected behavior is assumed to result from reduced flow separation which drove clockwise rotation. Contrary to the anticipated increase in separation-induced turbulence, the turbulence reduced the flow separation resulting in a low rotational response for velocities in the range of 15-25 m/s. Notably, the analysis indicates that under standard wind conditions (0-25 m/s), the tilt response due to wind loading is minimal, not exceeding 1°. This finding has significant implications for the design and operation of floating PV systems in typical marine environments.

It was observed that changing the wind direction reduced the rotational response of the module. This was also contrary to expectation as the drag forces experienced by the module in reverse orientation were higher than those in the forward orientation. Although the forces experienced by the device in the horizontal and vertical direction are found to be higher, due to the nature of the flow around the device, the net moment is lower. Therefore, the module is more prone to rotation when wind acts in the panel-facing direction which exerts higher mechanical loading on the PV panel as well. Both of these factors make the wind loading in the frontal direction critical in an environmental load analysis.

The behavioural response due to design tilt variations is also a major component of the study and has yielded promising results. The design tilts studied were in the rotational direction and peak tilts were found to be affected by the design tilt of the device. As the design tilt is increased, the module that initially exhibits clockwise rotation at 0° slows tends to anticlockwise rotation which also peaks around 25°. The trend of increased anti-clockwise rotation can be found analogous to the rotational response observed with increasing flow velocities. Flow seperation at the leading edge is therefore strongly believed to be the reason for clockwise rotation and limiting this phenomenon could be beneficial to curbing wind-induced tilting observed in PV modules. Based on the simulation results, a small tilt of under 10° could be beneficial in reducing module tilt variation under wind loading in normal operating conditions.

Based on the parametric study on the floater height, it is also seen that increasing the height of the device has a significant effect on the tilt variation of the device and it becomes a critical factor in the design process. An increase in the floater height by 20 cm causes an increase in tilt by 2° for an FPV module with a 24° geometric tilt. Optimising the height of the floater could help minimise movement losses. It also could be useful to increase the mass of the bottom part of the floater for the same height which would bring down the center of gravity of the device and lower the motion response.

## 5.2 Accuracy of results

It is important to understand how verifiable or accurate these results are before proceeding to use them as an assessment tool. Although wind tunnel tests or similar experimental testing is the best method to validate the results, this is out of the scope of this thesis.

The general movement of the FPV device in the simulations is varied, however, they follow some general similarities in movement. This is detailed in Chapter 4. These characteristics indicate that the rotational movement of the device is affected by hydrodynamic damping and the inertia of the device.

A simplified analytical model will be used to check if the results for obtained tilt variation are within the range of what is expected for the system. Since the CFD studies are done on a dynamic model, this analytical simplification might be erroneous to use for the entire response. Therefore it will be used to compare the maximum tilt obtained from each simulation.

### 5.2.1 Analytical Model

The analytical model is primarily used to confirm if the range of motion of the body simulated under wind loading can be verified. For this purpose, an averaged rotational moment around the z-axis acting on the body will be provided to the body. This averaged value will be based on the recorded values of the moment on the FPV device from the simulation such as in Figure 4.16.

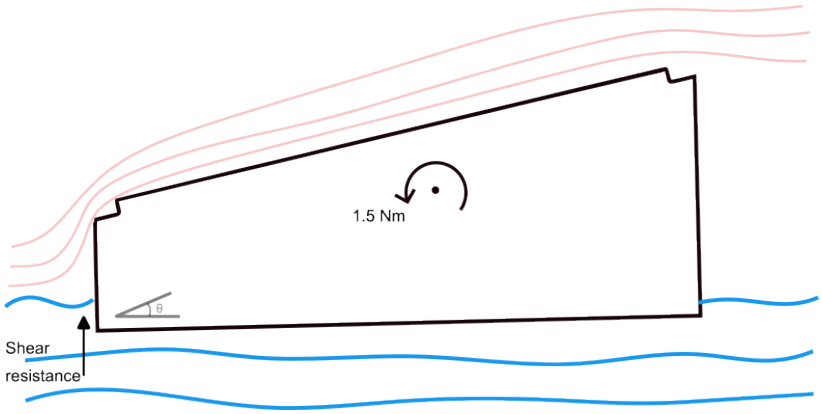


Figure 5.2: Illustration of FPV module rotation on the surface of water considering rotational moment and shear resistance of water.

An illustration of the model is shown in Figure 5.2. For the rotation of the FPV module, the primary hindrance is assumed to be the shearing of water during rotation and the corresponding drag applied on the module. Drag force can be calculated using Equation 5.1

$$F_{drag} = C_d \cdot 0.5 \cdot \rho \cdot (r \cdot \omega)^2 \cdot A_s \tag{5.1}$$

where,

- $C_d$ is 1.05 for hexahedral shapes [82].
- $A_s$ is the area of the body submerged under water, $A_s$ = 0.9718 $m^2$,
- $r$ is the radius of rotation of the body, $r$ = 0.5492 $m$,
- $\rho$ is the density of water, $\rho$ = 998.2 $kg/m^3$,
- $\omega$ is the angular velocity of the body in water.

Using the relation $M = I \cdot \alpha$ we can relate the moment force acting on the body to the rotational movement of the body. The maximum moment force acting on an FPV module with 12° tilt and 40 m/s wind acting on is around 1.5 Nm and the drag force assumed to act at the midpoint of the moment arm is assumed to provide restoring torque. When incorporating this into the relation, we get

$$I \cdot \frac{d\omega}{dt} = M - \left((0.5 \cdot r) \cdot C_d \cdot 0.5 \cdot \rho \cdot (r \cdot \omega)^2 \cdot A_s\right)$$

Solving this equation and applying initial conditions, a relation to the initial tilt is obtained in the form:

$$\theta = 0.188 \cdot ln(\frac{1 + e^{-5.383t}}{2}) \implies \lim_{t \to \infty} \theta = -1.29^\circ$$

The negative sign in the analytical solution suggests the sign convention used with anti-clockwise movement being negative. Considering this, the tilt angle provided by this analysis is close to the 1.5° peak tilt obtained through the solution. The match indicates that the obtained solutions are within the range of physical probability.

### 5.2.2 Numerical errors

During the study, it was observed that there was a significant change in the simulation behaviour when the convergence criteria and the time step were varied. In particular, the simulation settings for the wind speed variation were very computationally intensive while a more relaxed simulation setting for the geometric tilt variation was much more computationally affordable.

The differences of the two simulations are listed below:

- Simulation 1, Sim-1 (wind speed variation): Variable time step (Courant No: 0.1 - 1, time step (1e-4 - 0.005)) and residuals $< 10^{-5}$.
- Simulation 2, Sim-2 (design tilt variation): Fixed time step ($\Delta t$: 0.001) and residuals ¡ $10^{-3}$.

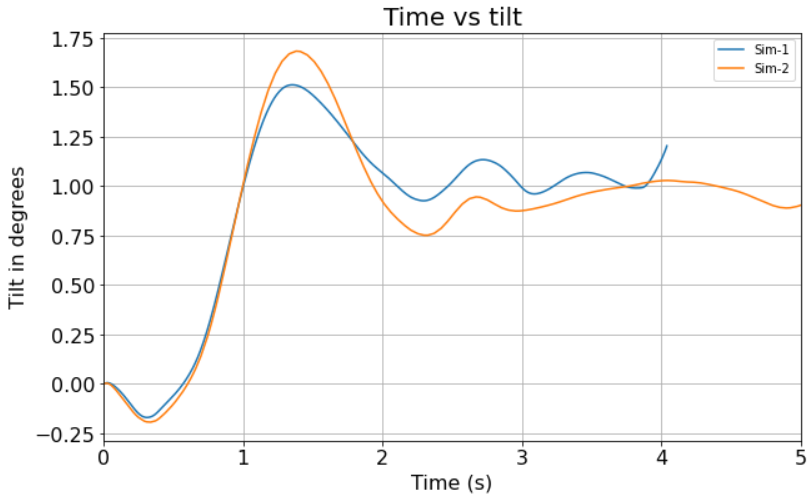


Figure 5.3: Difference in rotational response in Simulation 1 and Simulation 2.

The relaxed settings improved the calculation speed by 400% and it was possible to simulate 10 s of motion instead of 5 s. However, from Figure 5.3, it can be seen that there is a numerical difference in the computation of the result. The peak rotational angle is higher for the second simulation by 0.17° which is a 10% error. In addition, the dynamic response behaviour is also different with Simulation 1 having more frequent peaks.

The differences in these simulations only highlight the nature of the solutions that are computed. The numerical accuracy of the response behaviour cannot be easily referenced and validated as this is a new field of study. Hence, the simulation studies performed can be used as a methodological approach to get an idea of the response behaviour but experimental validation is required to fully understand the complexity of the motion.

## 5.3 Suitability of CFD for FPV performance assessment

### 5.3.1 Effects on PV yield

Previous sections indicate how the tilt of the PV might be affected by the wind loading. As mentioned in Chapter 1, the PV tilt variations can be coupled with other climate-related computations such as irradiance and temperature computations that help estimate PV yield for a longer period.

For the scope of this work, due to computational and time limitations, we will limit the study of the effects on PV performance to a single case study. The tilt response used in this performance check is the 5 s tilt response from the simulation study and is assumed to be the equilibrium tilt response. Low wind velocity tilt responses from the numerical study display close to linear decay and converge well within the time frame of the simulation. Therefore

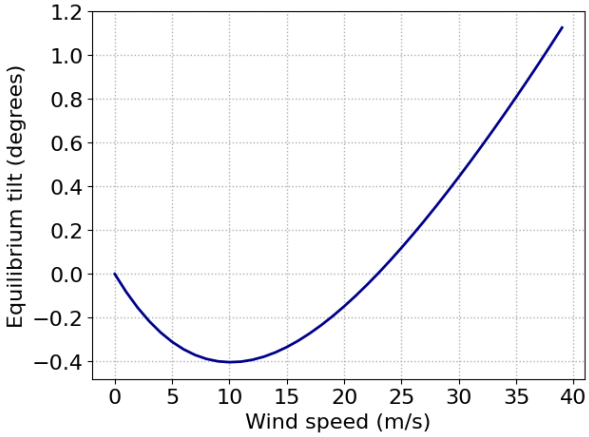


Figure 5.4: Equilibrium tilt variation of the FPV in response to different wind speeds.

this assumption is valid for low-velocity conditions of 0-15 m/s will be considered in this study. The tilt variation data from the study were fit into a fourth-degree polynomial curve that matched the simulation output. This can be seen in Figure 5.4. The PV panel used for the yield assessment comparison is the 365W-rated 'TSM-DE14A (II) PERC MONO' panel from Trinasolar. The dimensions of the module match the PV panel assumed in the simulation study. PV characteristics of the module are mentioned in Table 5.1.

| Characteristic | Value |
|---|---|
| $T_{NOCT}$ | 44± 2°C |
| $P_{max}$ temperature coefficient | -0.39%/°C |
| $T_{STC}$ | 25°C |
| $P_{STC}$ | 365( +5) W |
| $v_{STC}$ | 18.88% |
| Module dimensions | 1960 × 992 × 40 mm (77.2 × 39.1 × 1.57 inches) |
| Weight | 26kg |

Table 5.1: Specifications of PV module [17].

An hour of weather data is considered and the difference in the power generation when the movement of the panel is checked. The weather data was obtained as 10-minute resolution data from the meteorological institute KNMI. The irradiance, temperature, and wind speed data is collected from the station location 53.3911°$N$ and 5.3458°$E$ near IJsselmeer. The station data on the date 24-4-2022 and the time between 11:00 and 12:00 is used for this calculation. The irradiance data from the station is received initially as only GHI (Global Horizontal Irradiance) data but is processed with the help of the BRL decomposition model [83, 84] to obtain DNI (Direct Normal radiance) and DHI (Diffuse Horizontal Irradiance) values. The DNI, DHI, GHI, and ambient temperature are converted to 10 s resolution data through linear interpolation. Figure 5.5 shows the irradiances used in the calculations. Solar

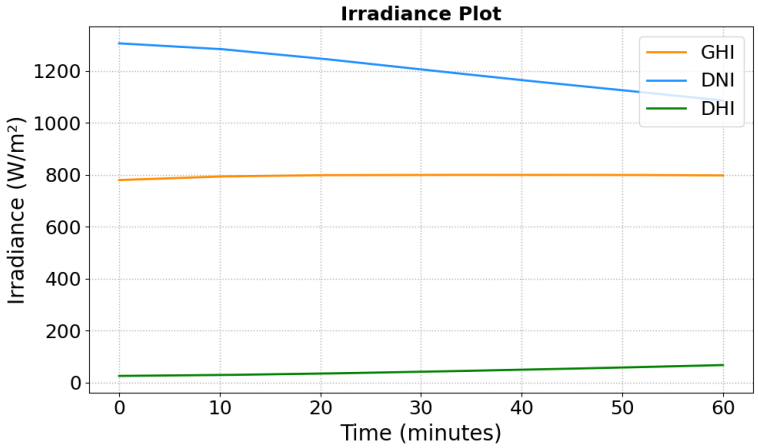


Figure 5.5: Irradiance values used in the yield assessment model.

position data is acquired using the PVlib python package.

Next, the mean wind speed data obtained at 10-min resolution is converted to a more realistic wind profile. The wind speed profile is as shown in Figure 5.6. Since the simulation study has been conducted for a period of 10 s, high-frequency wind spectra that model gust variations were chosen to create the wind profile. The wind spectra that best fit the high-frequency criteria is found to be the Harris spectra which is typically used for wind flow over land (in reality, the wind over water has a much lower frequency due to low obstructions and is more accurately represented by the Froya wind spectrum which uses hourly mean wind speed data) [12]. Appendix D shows the calculations done to obtain the wind speed profile.

This function is then used to change the module inclination. Positive rotational tilt is assumed

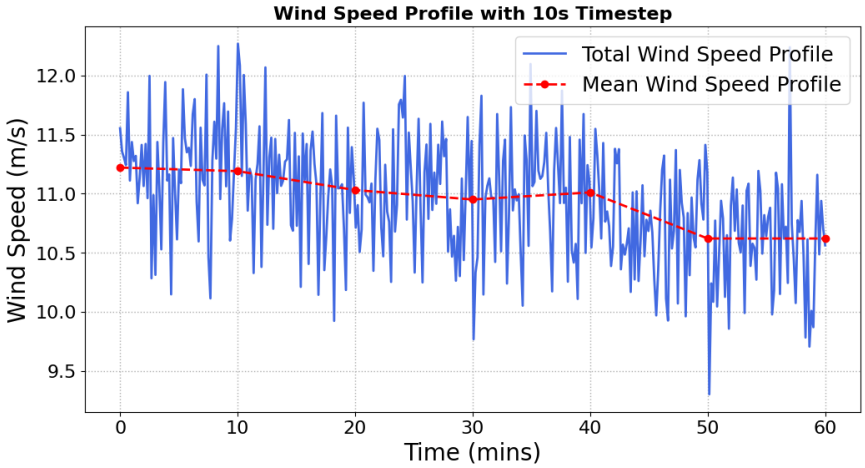


Figure 5.6: Mean and complete wind speed profile of the PV yield study.

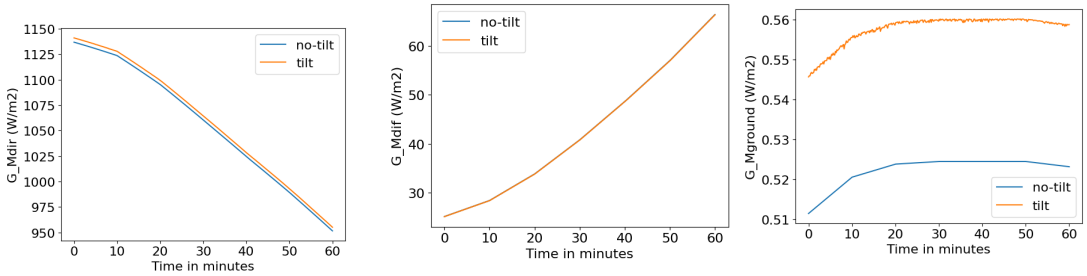


(a) Variation in direct irradiance.

(b) Variation in diffuse irradiance.

(c) Variation in reflected irradiance.

Figure 5.7: Variation in irradiance on the module due to the inclusion of wind-induced tilt.

to be in the anticlockwise direction which increases the module tilt angle and vice versa for the anti-clockwise direction. The changes in the Angle of Irradiance (AOI) of the module affect the direct, diffuse, and reflected components of irradiation. An isotropic diffuse sky model was assumed to compute DHI [85], while the albedo of water was assumed as 0.06 for the open ocean [86]. The variation in irradiance for each component is shown in Figure 5.7.

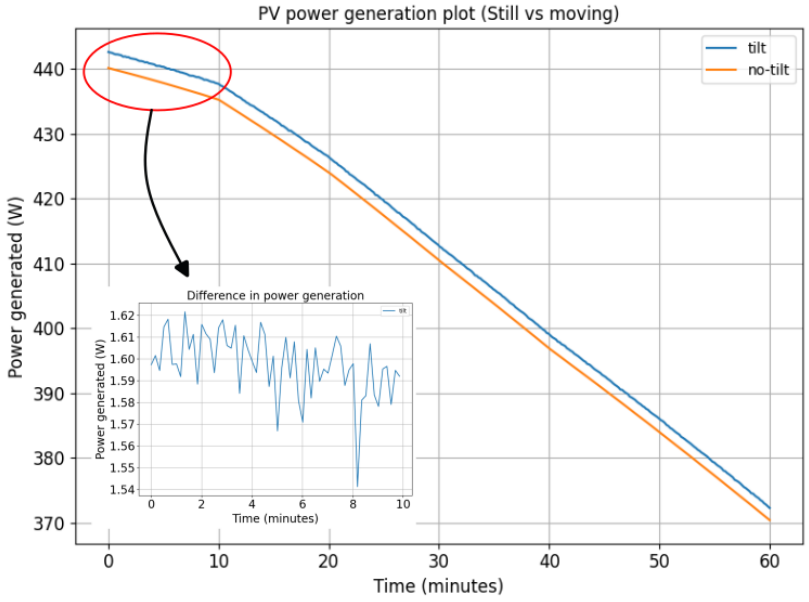


Figure 5.8: Power generation plot with the tilt variations (blue) and without (yellow).

From Figure 5.7a, a slight increase in the direct irradiation is observed when tilt is considered in yield evaluation. There is no corresponding change in the diffuse irradiance and although the difference in reflected irradiance is noticeable in Figure 5.7c, it has no significant impact on the total irradiance on the module. The yield calculations are simplified and include only the direct PV yield changes due to temperature and irradiance effects. The Duffie-beckman thermal model [87, 88] is used to calculate temperature effects on the module. The difference

in power output for the given weather conditions is seen in Figure 5.8. The power output per second changes in the range of 1.3 - 1.6 W for the duration of the study.

From Figure 5.8, it is noted that there are small variations in yield for the full hour of the study. It is also observed that the effect of the wind speed variations on the yield is proportional to the irradiation. It would be interesting therefore to investigate the sensitivity of tilt variation for different irradiance conditions. However, since the net difference in energy yield comes to only 0.4% of the standard PV yield, it would not be useful to spend high computational effort to calculate tilt variations in the module.

## 5.4 Summary

This chapter discusses the results from Chapters 3 and 4, and summarises the most important aspects of the CFD analysis. A brief description is provided on the importance of flow separation in the simulated tilt of the FPV and how these results will be useful for the design of the module. Later, an analytical check was performed to check the validity of the results obtained from the simulation. The tilt angles obtained from the analytical model were found to have good agreement with the numerical results. The numerical errors in the simulation were also investigated and the variation in the rotational peaks observed for the two simulations is found to be 10% and the dynamic response is found to be different as well. Hence, it is recommended to perform experimental checks before proceeding with a numerical approach. Finally, a PV yield analysis is done incorporating the tilt variations due to velocity as a polynomial fit. The wind loading is found to affect the yield of the module at a greater proportion when the irradiance is higher. However, the net effect of the inclusion of tilt in the yield model is found to cause a net change of less than 0.5%. The computational effort required for the calculation of the tilt variations is therefore not found to be justified.

**Is the methodology used in this thesis a useful tool for FPV performance assessment?**

Through this study, a CFD methodology was built to analyze the FPV system response to changes in tilt induced by wind loading. It is highlighted through different simulation studies although CFD provides valuable information about wind flow behaviour around a floating PV module, the numerical accuracy is still uncertain. The accuracy of the solutions obtained needs to be tested and validated to move forward and understand the exact nature of the methodology required.

From the accuracy, complexity of analysis, and computational efforts required for CFD analysis, it is determined that CFD can only be a supplementary tool to experimental studies that analyze wind effects. Thus, the methodology in its current form is not a useful tool for FPV performance assessment. In addition, due to the insignificant change in PV performance, it is also recommended to do experimental studies on FPV systems containing multiple PV panels before depending on CFD as a performance assessment and monitoring tool.

# 6 Conclusion

This chapter summarises the answers to the research questions, concludes the thesis work, and provides recommendations for future research.

## 6.1 Research Questions

This section summarises the research findings by answering individual research questions.

1. **The chosen methodology for evaluating wind loading on offshore floating PV:**

   The literature study identified a lack of experimental data and reliable field data on wind loading for offshore floating PV (FPV) systems. As analytical studies are also found to be not viable, a numerical approach is chosen as the best evaluation methodology. Among the tools available for assessing wind response, Computational Fluid Dynamics (CFD) was determined to be the most suitable for this study. Drawing from contemporary studies, a simplified methodology was developed to numerically determine the tilt variation of an FPV system. The numerically determined tilt, if feasible, is proposed to be then combined with wave-induced tilt. This combined tilt variation would then be incorporated into the current FPV performance assessment methodology. Based on the available FPV designs, three relevant FPV geometries—tubular float, individual raft, and platformed systems—were identified as potential FPV archetypes for marine deployment.

2. **Wind Flow Behavior Around a PV Module:** Wind flow over a stationary PV panel is investigated using 2D and 3D models. The models are validated with literature for drag and lift coefficients at varying tilt angles. The model studies reveal that static pressure significantly affects the leading edge of the PV panel, while dynamic pressure forces dominate the trailing edge. Since both edges of the panel are not uniformly affected by forces, the rotational movement is thought to be dependent on the nature of the flow more than the magnitude of the forces acting on it. Transient flow analysis is hence inferred to be important to analyse the tilt variation of the module. When the floater geometry is added to the PV panel geometry, maximum pressure is observed on the upwind side of the system. In addition, due to the variation in flow behaviour with tilt

angle change, forces become difficult to predict if rotation occurs, warranting further investigation through CFD studies.

3. **Tilt Variation of an FPV Module Exposed to Wind**:

   Simulations showed for wind-induced rotation of the FPV, the magnitude, and direction depend on flow separation at the leading edge. The highest rotational response of 4.07° (anticlockwise) was observed for a design tilt of 24° and a wind velocity of 40 m/s. Small design tilts of 5-10 degrees are found to be beneficial to minimize flow separation for normal wind conditions and minimize FPV rotation. Critical CFD model settings—spatial solver, time step, and mesh movement—were identified as crucial for accurate simulations. Parametric studies demonstrated that wind velocity and design tilt proportionally increase anticlockwise rotation, while the height of the floater's shorter side has the biggest influence on flow behaviour and rotational movement.

4. **Usefulness of the Methodology**:

   The study established a CFD-based methodology to analyze FPV system responses to wind-induced tilt variations. This methodology proved useful for understanding wind effects and identifying critical design parameters. Since the numerical errors during measurement could not be referenced nor the model validated, the limitations of CFD as a standalone tool are highlighted. The need for experimental validation and the significant computational effort involved suggest that CFD should be used alongside experimental studies, especially for more complex, interconnected FPV systems. After conducting a PV yield assessment including the variations in tilt due to wind loading, it is found that the variations change the total yield of the module by only 0.4%. The insignificant variation in yield urges further investigation of wind loading in tandem with wave loading before proceeding with this methodology.

### 6.1.1 Conclusions

This thesis explored the complexities of evaluating wind loading on offshore floating PV (FPV) systems, ultimately proposing a numerical methodology as the most viable approach in the absence of extensive experimental data. Computational Fluid Dynamics (CFD) analysis emerged as a powerful tool for understanding wind flow behaviour and predicting the rotational response of FPV modules to various wind and geometric parameters. However, the research also underscores the limitations of relying solely on CFD, particularly due to the computational intensity and the need for further validation through experimental studies.

The findings emphasize the importance of understanding the interaction between wind forces and FPV geometries, as well as the need for detailed parametric studies to optimize FPV design for offshore conditions. While CFD offers valuable insights, its efficacy as a performance assessment tool for FPV systems hinges on two critical factors: it's capacity to analyze more complex, interconnected FPV designs, and its ability to integrate wave-induced dynamics with wind-loading effects in an assessment framework.

Overall, this research contributes to the growing body of knowledge on FPV systems, offering a foundational methodology for future studies and highlighting areas where further investigation is necessary to enhance the reliability and performance of offshore floating PV installations.

## 6.2 Recommendations for future work

As a developing technology, there exists a lot of scope for wind loading studies for FPV systems. This thesis aims to deliver a comprehensive methodology for wind load analysis and to find its benefits. Future works could do the following to further the work:

1. Experimental validation: Although some parametric studies are done in this work since the work is novel and fully numerical there is no real-world behaviour to correlate the output with and validate the results. This creates a situation where it becomes difficult to move further with the results at hand. Hence, it is advised to perform experimental simulations that can be correlated with the current work so that a better confidence of the current results is obtained.
2. Improved computational power: It was noted in this study that CFD is a computationally intensive tool. Quite a bit of system memory is required for the system simulations, hence at least 32 GB of system RAM and 4.0+GHz CPU is required. To run simulations for longer periods or more complex geometries, it is suggested to use remote server access, cloud computing, or campus servers.
3. Simulation of multiple bodies and different designs: Due to time and computational constraints, it was not possible to simulate PV rows or arrays. It is much more beneficial to assess a PV array response as compared to an individual system response. Not only does it pose a more realistic scenario to include multiple PV modules but more complex system behaviour such as shading and shielding effects which affect the layout of a PV array can also be investigated. This analysis can be extended to consider different designs that currently exist in the market as well
4. 3D study: There are a variety of effects relating to turbulence and edge effects that are simplified with 2D models. 3D model investigations could give more insight into what effects are important in the assessment of wind loading on a PV module and also serve as a check to the current study.
5. Combining with wave model: Wind loading does not affect a floating body in isolation but rather in combination with wave and current effects. Wind-induced waves are also a major affector in this vein. Therefore, it is recommended to combine the current aerodynamic model with a hydrodynamic model to assess the complex system response to environmental loading.

# Bibliography


[1] International Renewable Energy Agency, "Global trends in renewable energy," July 2024. https://public.tableau.com/views/IRENARETimeSeries/ExploreDashboard?:embed=y&:sid=&:redirect=auth&:toolbar=n&:display_count=n&:origin=viz_share_link.

[2] J. Lovering, M. Swain, L. Blomqvist, and R. R. Hernandez, "Land-use intensity of electricity production and tomorrow's energy landscape," *PLOS ONE*, vol. 17, p. e0270155, July 2022.

[3] N. Lee, U. Grunwald, E. Rosenlieb, H. Mirletz, A. Aznar, R. Spencer, and S. Cox, "Hybrid floating solar photovoltaics-hydropower systems: Benefits and global assessment of technical potential," *Renewable Energy*, vol. 162, pp. 1415–1427, Dec. 2020.

[4] S. Z. Mirbagheri Golroodbari *et al.*, *The Sun is rising over the North Sea: Assessment of offshore solar photovoltaics*. PhD thesis, Utrecht University, 2021.

[5] R. Cazzaniga, "Chapter 4 - floating pv structures," in *Floating PV Plants* (M. Rosa-Clot and G. Marco Tina, eds.), pp. 33–45, Academic Press, 2020.

[6] Junko Movellan, "Running out of precious land? floating solar pv systems may be a solution." https://www.renewableenergyworld.com/solar/running-out-of-precious-land-floating-solar-pv-systems-may-be-a-solution/, July 2013. Accessed: 2024-20-03.

[7] Oceans of Energy, "A world's first: offshore floating solar farm installed at the dutch north sea." https://oceansofenergy.blue/2019/12/10/a-worlds-first-offshore-floating-solar-farm-installed-at-the-dutch-north-sea-2/, Dec. 2019. Accessed: 2024-20-03.

[8] A. Honaryar, M. Karimirad, A. Abbasnia, and T. Whittaker, "Wind parameters effects on floating solar array design–case study: Japan's largest floating solar array," in *International Conference on Offshore Mechanics and Arctic Engineering*, vol. 85932, p. V008T09A008, American Society of Mechanical Engineers, 2022.

[9] C. Jubayer and H. Hangan, "Numerical simulation of wind loading on photovoltaic panels," in *Structures Congress 2012*, pp. 1180–1189, 2012.

[10] O. Mursid, O. Mursid, K. R. Malau, K. R. Malau, N. Huda, N. Huda, A. M. A. Abidin, A. M. A. Abidin, G. Sutarno, and G. Sutarno, "Design and feasibility studies a floating photovoltaic to supply electricity for isolated island village in indonesia," *null*, vol. 698, p. 012033, Mar. 2021.

[11] S. M. Choi, C.-D. Park, S.-H. Cho, and B.-J. Lim, "Effects of various inlet angle of wind and wave loads on floating photovoltaic system considering stress distributions," *Journal of Cleaner Production*, 2023.

[12] DNV, "Dnv-rp-0584 design, development and operation of floating solar photovoltaic systems. dnv standards for offshore solar pv," 2021.

[13] V. E. Uslu, "Computational fluid dynamic analysis of wind loads acting on ground mounted solar panels," Master's thesis, Middle East Technical University, 2014.

[14] A. T. Giorges, G. J. Amador, K. Caravati, and J. Goodman, "Numerical simulation of aerodynamic force on solar panels," in *ASME International Mechanical Engineering Congress and Exposition*, vol. 56284, p. V06AT07A059, American Society of Mechanical Engineers, 2013.

[15] S. Mohapatra, "Wind tunnel investigation of wind load on a ground mounted photovoltaic tracker," Master's thesis, Colorado State University, 2011.

[16] M. Shademan and H. Hangan, "Wind loading on solar panels at different inclination angles," in *11th Americas conference on wind engineering*, pp. 22–26, San Juan Puerto Rico, 2009.

[17] TrinaSolar, "Tallmax plus," 2018. Accessed: 2024-08-18.

[18] Ember-Climate. https://ember-climate.org/insights/research/global-electricity-review-2023/, 2023. Global Electricity Review 2023, License: CC BY 4.0.

[19] S. E. Weart, "The carbon dioxide greenhouse effect," May 2023.

[20] W. Bach, "Fossil fuel resources and their impacts on environment and climate," *International Journal of Hydrogen Energy*, vol. 6, no. 2, pp. 185–201, 1981.

[21] N. Mimura, "Sea-level rise caused by climate change and its implications for society," *Proceedings of the Japan Academy, Series B*, vol. 89, no. 7, pp. 281–301, 2013.

[22] H. Visser, "The significance of climate change in the netherlands," *An analysis of historical and future trends (1901–2020) in weather conditions, weather extremes and temperature-related impacts. MNP report*, vol. 550002007, 2005.

[23] J.-C. Ciscar, A. Iglesias, L. Feyen, L. Szabó, D. Van Regemorter, B. Amelung, R. Nicholls, P. Watkiss, O. B. Christensen, R. Dankers, L. Garrote, C. M. Goodess, A. Hunt, A. Moreno, J. Richards, and A. Soria, "Physical and economic consequences of climate change in europe," *Proceedings of the National Academy of Sciences*, vol. 108, pp. 2678–2683, Jan. 2011.

[24] N. Gaulin and P. Le Billon, "Climate change and fossil fuel production cuts: assessing global supply-side constraints and policy implications," *Climate Policy*, vol. 20, no. 8, pp. 888–901, 2020.

[25] IEA. https://www.iea.org/data-and-statistics/charts/renewable-electricity-capacity-additions-by-technology-and-segment-2016-2028, 2023. Renewable electricity capacity additions by technology and segment, 2016-2028, IEA, Paris; License: CC BY 4.0.

[26] T. A. Troszak, "The hidden costs of solar," *Energy Highlights*, 2021.

[27] D.-J. van de Ven, I. Capellan-Peréz, I. Arto, I. Cazcarro, C. de Castro, P. Patel, and M. Gonzalez-Eguino, "The potential land requirements and related land use change emissions of solar energy," *Scientific Reports*, vol. 11, Feb. 2021.

[28] I. Capellán-Pérez, C. de Castro, and I. Arto, "Assessing vulnerabilities and limits in the transition to renewable energies: Land requirements under 100

[29] UNFPA. https://www.unfpa.org/world-population-trends, 2023. United Nations Population Fund-World Population Trends, License: CC BY 4.0.

[30] EIA. https://www.eia.gov/outlooks/ieo/, 2023. International Energy Outlook 2023, U.S Energy Information Administration, License: CC BY 4.0.

[31] M. Scheepers, A. Faaij, and R. Van den Brink, "Scenarios for a climate-neutral energy system; smart combinations of energy options lead to sustainable and affordable energy management," 2020.

[32] N. Nederland. https://www.netbeheernederland.nl/publicaties-en-codes/publicaties, 2023. Transition of the Dutch energy system: scenario's 2030-2050, II3050 Management Summary.

[33] Solarplaza. https://www.solarplaza.com/resource/11814/10-percent-dutch-agricultural-land-required-solar-parks/, 2018. The solar future NL, Published on:5 April 2018.

[34] R. Quax, M. Londo, W. van Hooff, T. Kuijers, J. Witte, W. van Sark, and W. Sinke, "Assessment of spatial implications of photovoltaics deployment policies in the netherlands," *Solar Energy*, vol. 243, pp. 381–392, Sept. 2022.

[35] G. of the Netherlands. https://www.government.nl/documents/reports/2019/06/28/climate-agreement, 2019. Climate Agreement, The Hague, 28 June 2019.

[36] N. E. Agency. https://english.rvo.nl/topics/offshore-wind-energy/plans-2030-2050, 2021. Offshore Wind Energy Plans 2030-2050, Published on:19 July 2021.

[37] S. Golroodbari, D. Vaartjes, J. Meit, A. van Hoeken, M. Eberveld, H. Jonker, and W. van Sark, "Pooling the cable: A techno-economic feasibility study of integrating offshore floating photovoltaic solar technology within an offshore wind park," *Solar Energy*, vol. 219, pp. 65–74, May 2021.

[38] L. Holthuijsen, Y. Eldeberky, N. Booij, and P. Ferier, "The maximum significant wave height in the southern north sea," Feb 1995.

[39] R. Nagananthini, R. Nagavinothini, and P. Balamurugan, "Floating photovoltaic thin film technology—a review," *Intelligent Manufacturing and Energy Sustainability: Proceedings of ICIMES 2019*, pp. 329–338, 2020.

[40] DNV, "Design, development and operation of floating solar photovoltaic systems, dnvgl-rp-0584." Electronic, Mar. 2021.

[41] H. Z. Maria Ikhennicheu, Alba Alcañiz Moya, "Guidelines for design, procurement and om friendly concepts for floating pv," Task report 2.4, INNOSEA, Mar. 2023.

[42] N. Wemekamp, "Systematic approach to find a suitable floating pv-structure on a given location: Comparing the environmental loads on different types of floating solar structures," 2023.

[43] M. Ikhennicheu, M. Ikhennicheu, B. Danglade, B. Danglade, R. Pascal, R. Pascal, R. Pascal, R. Pascal, V. Arramounet, V. Arramounet, Q. Trébaol, Q. Trébaol, F. Gorintin, and F. Gorintin, "Analytical method for loads determination on floating solar farms in three typical environments," *Solar Energy*, 2021.

[44] A. Sahu, N. Yadav, and K. Sudhakar, "Floating photovoltaic power plant: A review," *Renewable and sustainable energy reviews*, vol. 66, pp. 815–824, 2016.

[45] W. S. M. Water, "Floating solar handbook for practitioners," *World Bank Group, ESMAP, SERIS*, 2019.

[46] K. Trapani and M. Redón Santafé, "A review of floating photovoltaic installations: 2007–2013," *Progress in Photovoltaics: Research and Applications*, vol. 23, pp. 524–532, Jan. 2014.

[47] S. Patil Desai Sujay, M. Wagh, and N. Shinde, "A review on floating solar photovoltaic power plants," *Int. J. Sci. Eng. Res*, vol. 8, pp. 789–794, 2017.

[48] G. Huang, Y. Tang, X. Chen, M. Chen, and Y. Jiang, "A comprehensive review of floating solar plants and potentials for offshore applications," *Journal of Marine Science and Engineering*, vol. 11, p. 2064, Oct. 2023.

[49] Ciel et Terre, "The synergy between the sunshine and the power of water." https://ciel-et-terre.net/floating-solar/, 2024. Accessed: 2024-08-18.

[50] W. Soppe, "Challenges and potential for offshore solar," tech. rep., TKI Wind op Zee, Feb. 2022.

[51] TNO, "Floating solar panels," 2022. Accessed: 2024-08-18.

[52] L. Micheli, "The temperature of floating photovoltaics: Case studies, models and recent findings," *Solar Energy*, vol. 242, pp. 234–245, 2022.

[53] N. A. Elminshawy, A. Osama, D. El-Damhogi, E. Oterkus, and A. Mohamed, "Simulation and experimental performance analysis of partially floating pv system in windy conditions," *Solar Energy*, vol. 230, pp. 1106–1121, 2021.

[54] S. Z. Golroodbari and W. van Sark, "Simulation of performance differences between offshore and land-based photovoltaic systems," *Progress in Photovoltaics: Research and Applications*, vol. 28, pp. 873–886, May 2020.

[55] S. Golroodbari and W. van Sark, "On the effect of dynamic albedo on performance modelling of offshore floating photovoltaic systems," *Solar Energy Advances*, vol. 2, p. 100016, 2022.

[56] H.-J. Joo, S.-J. Heo, S. Kim, and W. Choi, "Wind load distribution in float photovoltaic system," *Applied Sciences*, 2023.

[57] C.-R. Lee, G.-H. Lee, J.-Y. Shim, D.-H. Choi, and J.-H. Lee, "Structural safety evaluation through full modules analysis of 2 wm class floating photovoltaic power plant," *Journal of the Korean Solar Energy Society*, vol. 41, no. 6, pp. 109–118, 2021.

[58] D. Lungu, P. Van Gelder, and R. Trandafir, "Comparative study of eurocode 1, iso and asce procedures for calculating wind loads," *IABSE reports*, pp. 345–354, 1996.

[59] J. Cao, A. Yoshida, P. K. Saha, and Y. Tamura, "Wind loading characteristics of solar arrays mounted on flat roofs," *Journal of Wind Engineering and Industrial Aerodynamics*, vol. 123, pp. 214–225, 2013.

[60] D. E. Neff and R. N. Meroney, "Wind performance of photovoltaic arrays," 2003.

[61] A. M. Aly, N. A. M. Aly, J. Whipple, and N. J. Whipple, "Wind forces on ground-mounted photovoltaic solar systems: A comparative study," *Applied Solar Energy*, null.

[62] O. Bogdan and D. Creţu, "Wind load design of photovoltaic power plants by comparison of design codes and wind tunnel tests," *Mathematical Modelling in Civil Engineering*, vol. 15, pp. 13–27, Sept. 2019.

[63] M. T. Browne, Z. J. Taylor, S. Li, and S. Gamble, "A wind load design method for ground-mounted multi-row solar arrays based on a compilation of wind tunnel experiments," *Journal of Wind Engineering and Industrial Aerodynamics*, vol. 205, p. 104294, Oct. 2020.

[64] Z. Samani and Z. Samani, "Wind loading on full-scale solar panels," *null*, 2016.

[65] S. N. A. Yusuf, Y. Asako, N. A. C. Sidik, S. B. Mohamed, and W. M. A. A. Japar, "A short review on rans turbulence models," *CFD Letters*, vol. 12, no. 11, pp. 83–96, 2020.

[66] J. Sodja, "Turbulence models in cfd," *University of Ljubljana*, pp. 1–18, 2007.

[67] J. L. Suárez, J. L. L. Suárez, D. Cadenas, D. Cadenas, H. Rubio, H. Rubio, P. Ouro, and P. Ouro, "Vortex shedding dynamics behind a single solar pv panel over a range of tilt angles in uniform flow," *Fluids*, 2022.

[68] I. I. Sheikh, "Numerical investigation of drag and lift coefficient on a fixed tilt ground mounted photovoltaic module system over inclined terrain," *Int J Fluids Eng*, vol. 11, pp. 37–49, 2019.

[69] M. Shademan, R. Barron, R. Balachandar, and H. Hangan, "Numerical simulation of wind loading on ground-mounted solar panels at different flow configurations," *Canadian Journal of Civil Engineering*, vol. 41, no. 8, pp. 728–738, 2014.

[70] S.-J. Yoon, S. J. Yoon, S.-J. Yoon, H. J. Joo, H. J. Joo, S. H. Kim, S. H. Kim, and S. H. Kim, "Structural analysis and design for the development of floating photovoltaic energy generation system," *IOP Conference Series: Materials Science and Engineering*, 2018.

[71] Y.-G. Lee, Y.-G. Lee, H.-J. Joo, H.-J. Joo, S.-J. Yoon, and S.-J. Yoon, "Design and installation of floating type photovoltaic energy generation system using frp members," *Solar Energy*, 2014.

[72] S. M. Choi, S. M. Choi, G. R. Lee, G. R. Lee, C. D. Park, C. D. Park, S. H. Cho, S. H. Cho, B. J. Lim, B.-J. Lim, and B. J. Lim, "Wind load on the solar panel array of a floating photovoltaic system under extreme hurricane conditions," *Sustainable Energy Technologies and Assessments*, 2021.

[73] S.-H. Kim, S.-J. Yoon, and W. Choi, "Design and construction of 1 mw class floating pv generation structural system using frp members," *Energies*, vol. 10, p. 1142, Aug. 2017.

[74] G.-H. Lee, G.-H. Lee, G.-H. Lee, J. Choi, Choijiwoong, J. M. Seo, J.-W. Choi, H. Ha, HojinHa, J.-H. Seo, H. Ha, and H. Ha, "Comparative study of effect of wind and wave load on floating pv: Computational simulation and design method," *null*, 2019.

[75] K.-C. Su, P.-H. Chung, and R.-Y. Yang, "Numerical simulation of wind loads on an offshore pv panel: the effect of wave angle," *Journal of Mechanics*, vol. 37, pp. 53–62, 2020.

[76] J. D. Holmes, "Mean and fluctuating internal pressures induced by wind," in *Wind Engineering*, pp. 435–450, Elsevier, 1980.

[77] U. Manual, "Ansys fluent 12.0," *Theory Guide*, vol. 67, 2009.

[78] M. Z. Jacobson and V. Jadhav, "World estimates of pv optimal tilt angles and ratios of sunlight incident upon tilted and tracked pv panels relative to horizontal panels," *Solar energy*, vol. 169, pp. 55–66, 2018.

[79] F. Forsgren, "Simulations to determine the drag coefficient of a floating photovoltaic system," 2021.

[80] F. R. Menter, "Two-equation eddy-viscosity turbulence models for engineering applications," *AIAA journal*, vol. 32, no. 8, pp. 1598–1605, 1994.

[81] S. Lecheler, "Computational fluid dynamics," 2023.

[82] S. F. Hoerner, "Fluid dynamic drag, published by the author," *Midland Park, NJ*, pp. 16–35, 1965.

[83] J. Boland, J. Huang, and B. Ridley, "Decomposing global solar radiation into its direct and diffuse components," *Renewable and Sustainable Energy Reviews*, vol. 28, pp. 749–756, 2013.

[84] S. Mishra, H. Ziar, O. Isabella, and M. Zeman, "Selection map for pv module installation based on shading tolerability and temperature coefficient," *IEEE Journal of Photovoltaics*, vol. 9, no. 3, pp. 872–880, 2019.

[85] P. G. Loutzenhiser, H. Manz, C. Felsmann, P. Strachan, T. Frank, and G. Maxwell, "Empirical validation of models to compute solar irradiance on inclined surfaces for building energy simulation," *Solar Energy*, vol. 81, no. 2, pp. 254–267, 2007.

[86] R. E. Payne, "Albedo of the sea surface," *Journal of the Atmospheric Sciences*, vol. 29, no. 5, pp. 959–970, 1972.

[87] J. A. Duffie, W. A. Beckman, and N. Blair, *Solar engineering of thermal processes, photovoltaics and wind*. John Wiley & Sons, 2020.

[88] A. Smets, *Solar Energy*. London: Bloomsbury Publishing Plc, 2016. Description based on publisher supplied metadata and other sources.

# A Flow Seperation

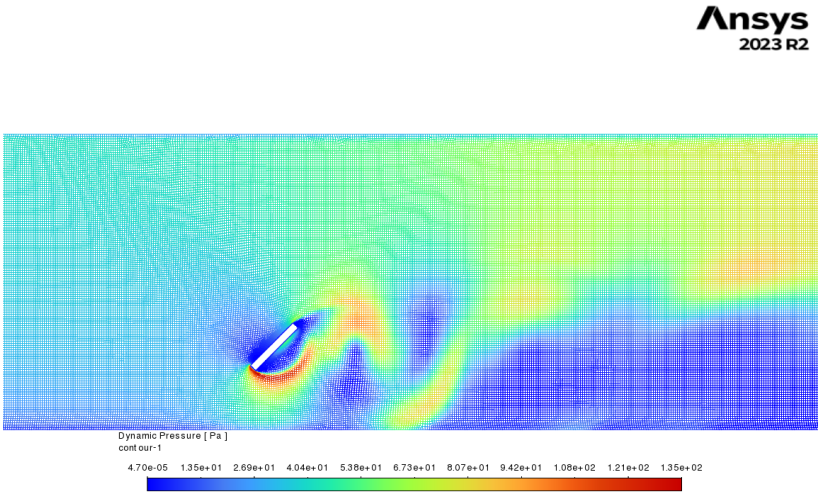


Figure A.1: 2D flow over a flat place at $\theta = 45°$.

Part of why it is difficult to analyze flow over PV panels is that the turbulence of the flow causes it to separate at the trailing edge and create a string of eddies downwind. An example of this was seen while running the transient analysis for flow over a 2D flat plate. The dynamic pressure contours are shown in Figure A.1. It can be seen that the trailing edge of the panel has a high dynamic pressure due to flow separation. This can also be seen in the turbulence contour (see Figure A.2) of the same. The separation-induced turbulence apart from delaying steady flow conditions also affects the resultant forces on the PV module and submits it to cyclical loading. Figure A.3 shows a zoomed in view of the cyclic forces acting on the PV panel in the 2D simulation in this transitional state. If not adequately designed for such loading, the vulnerable parts of the PV like the front glass might break. Due to the computational limitations of this thesis, the flow has been investigated only in the x-direction and for 5% turbulence. Increasing the flow speed and turbulence increases the occurence of this behaviour and it is good to investigate for PV design failure checks.

Surprisingly, the simulations for the PV with the floater geometry do not have this issue. The eddy formation downwind of the geometry is quickly dissipated to become a low-pressure

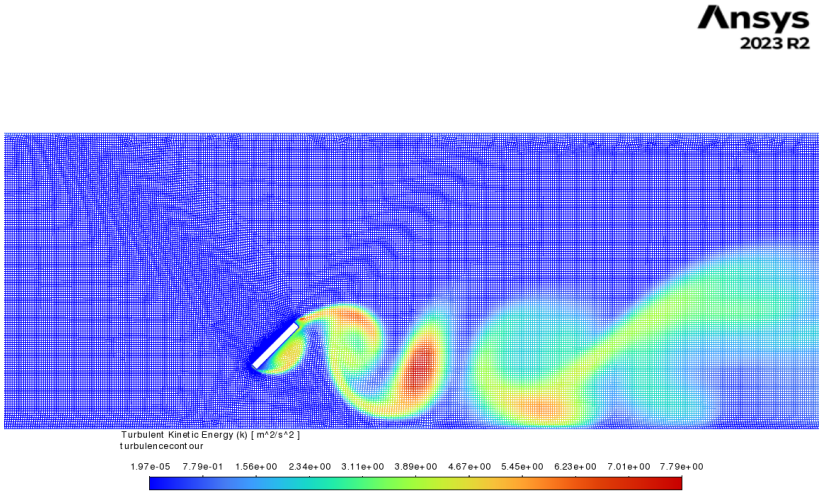


Figure A.2: Turbulence contour of flow separation in flow over a flat plate showing eddy formation in the downstream.

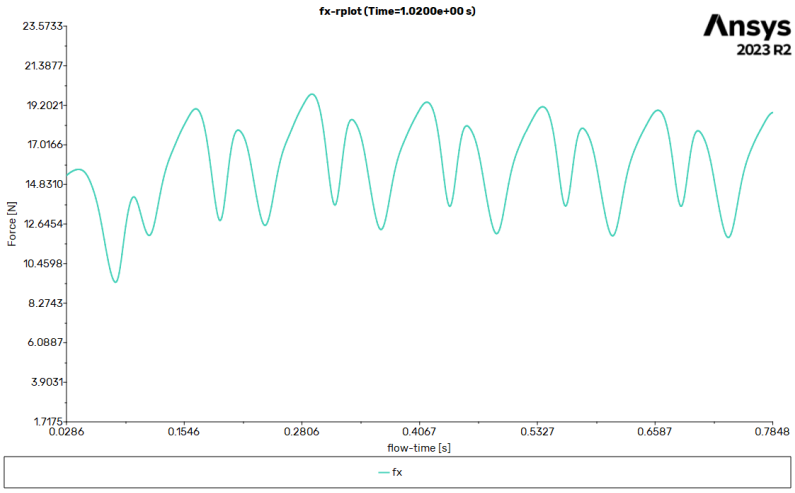


Figure A.3: Zoomed in view of x-directional cyclic force acting on a PV panel during a 2D wind flow study.

zone. This is possibly due to the presence of a boundary (wall-boundary in the case of single phase and air-water interface in the case of multi-phase) which does induce a boundary layer flow condition downstream. This may not be the case for very high velocities and may be a reason for irregular tilt angle variations observed for higher velocities in Section 4.2.1.

# B Other Validations

This appendix will detail the validations that were not included in the main thesis work. These will provide context into the assumptions made in the main study for the 3D model and the validation for 2D flat plate.

## B.1 3D flat plate mesh study

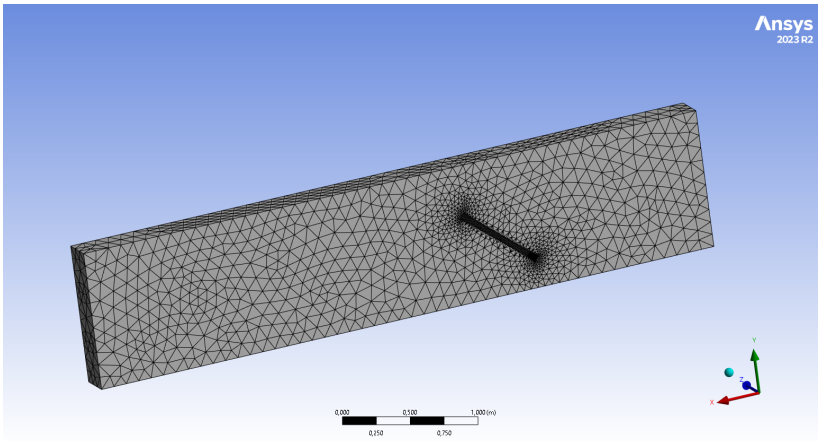


Figure B.1: 3D mesh setup used in the study.

Similar to the 2D flat plate mesh study, the same was conducted for 3D flat plate as well. The geometry and meshing of the 3D setup are shown in Figure B.1. When the simulation study was run for tetrahedral and hexahedral mesh of the same element size, the convergence of resulting force is as shown in Figure B.2. The tetrahedral curve shows greater variance when it comes to converges and converges a bit later as well. This also combined with taking almost double the computational cost makes hexahedral meshes the better choice of mesh element.

As part of the mesh study, the number of mesh elements also was checked against the steady state force in the x-direction. From Figure B.3, it is seen that the mesh elements currently used

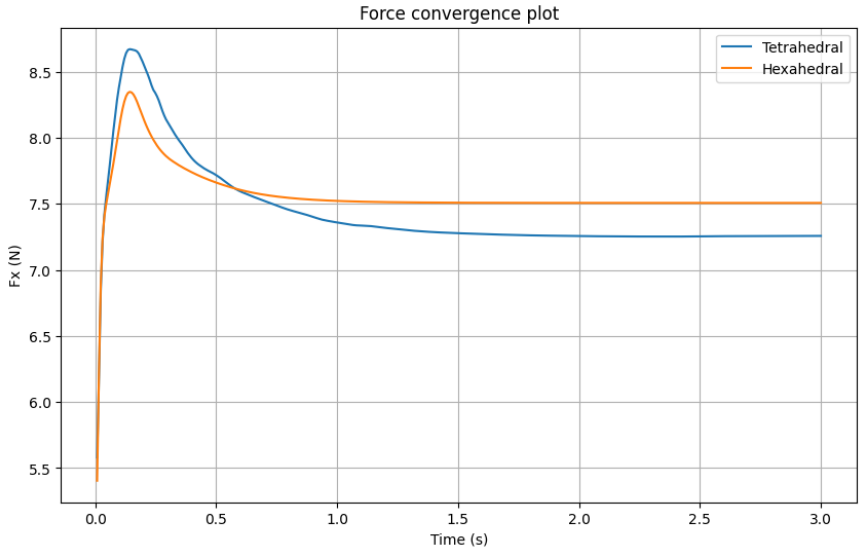


Figure B.2: Force convergence plot for 3D hexahedral and tetrahedral meshes.

is not sufficient for the accuracy of the solution. Comparing the results with the 2D solution as well, it becomes clear that increasing the mesh element count will lead to a more accurate solution. However, this increases the computational time by almost 3 fold for this simple case. Hence, it is found better to use 2D CFD studies for computational analysis.

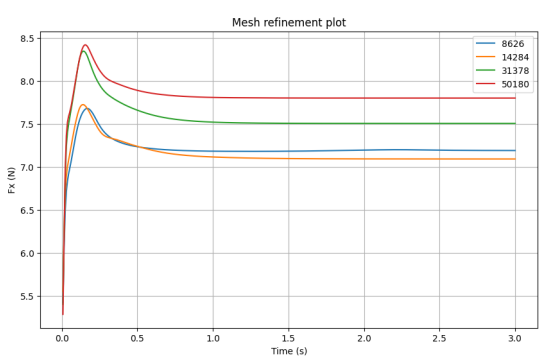


(a) Force comparison plot of 3D flat plate with different mesh element counts.

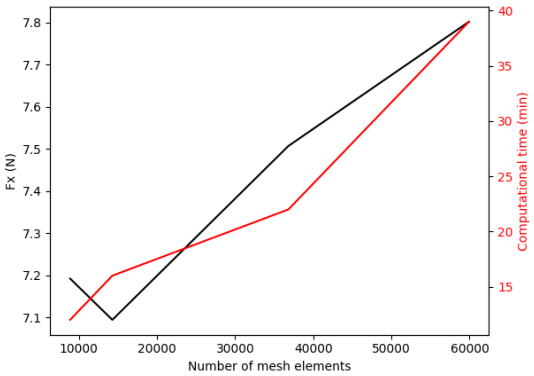


(b) Mesh refinement plot for 2D flat plate setup with computational time.

Figure B.3: Mesh study for 2D flow over a flat plate.

(a) Zoomed in view of the geometry and mesh of the FPV used in literature.

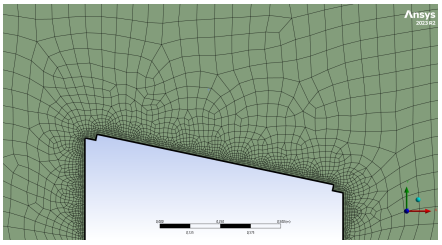


(b) Zoomed in view of the geometry and mesh of my FPV model.

Figure B.4: Meshes of the FPV module chosen.

## B.2 Cd for 2D FPV geometry

The drag coefficient across the floater was compared with the drag coefficient results by Forsgren *et al.* [79]. The simulation done by the reference literature used OpenFOAM and kept the module static. The monitored variables were the k value and the velocity profile. The geometry used by the literature is shown in Figure B.4a and the one simulated is in Figure B.4b.

The literature measured the drag coefficient for 0-50 m/s while my model simulated 10 m/s. The literature obtained a Cd value of 0.11 for the first FPV module in the array for their simulation. This value decreases slightly with an increase in velocity. This trend was observed for the flat plate simulation studies and well. The simulated study using Figure B.4b shows a Cd of 0.15. This slightly increased value can be due to the differences in mesh geometry. The velocity contours as seen in Figure B.5 however match the contours seen in literature and therefore the study can be said to show sufficient match with that of literature.

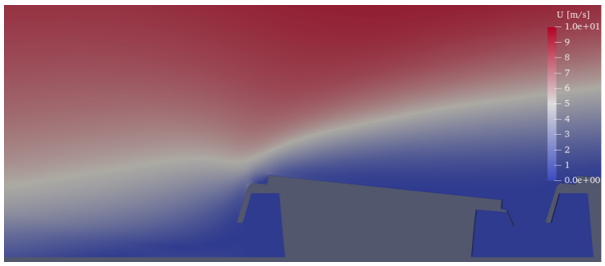


(a) Velocity contour over reference study.

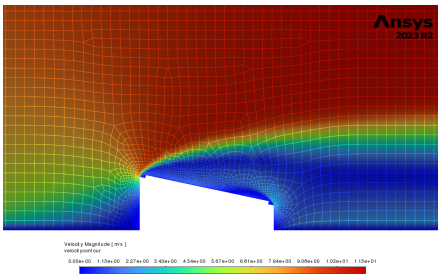


(b) Velocity contour over the FPV geomtery in my study.

Figure B.5: Velocity contours of the FPV module.

# C Floating Box Model

Before conducting a simulation study on the FPV geometry, a simulation study was done on a rectangular geometry to help set up the model. Most of the model control were tried out in this setup and the most suitable ones were chosen for the FPV geometry. Two of the most important settings that were finalised were that of the mesh settings and the time-step control.

Initially, a triangular element mesh was used to simulate the multi-phase flow since a dynamic mesh was utilised. To find the optimum number of mesh elements, a grid refinement analysis was done to determine the most optimal mesh size for the analysis. For this purpose, 1s simulations were run for multiple mesh elements with a velocity input of 10 m/s. The mesh refinement analysis looked at the tilt angle variation and the forces in the x and y direction acting on the FPV module. The results of the study is shown in Figure C.1

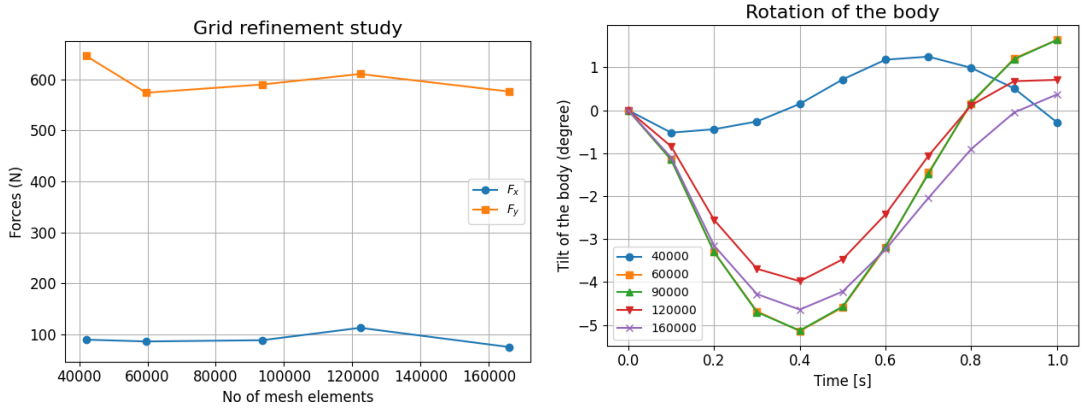


(a) Force comparison plot for different mesh sizes.

(b) Tilt variation comparison plot for different mesh sizes.

Figure C.1: Mesh study for multi-phase flow.

The Figure C.1a shows the force acting on the box in the x and y directions after 1 s of simulation. It is found to converge with increasing mesh elements but the variation in force is only slight. The variation of tilt angle in Figure C.1b is much more prominent for lower angles such as in 40000 mesh elements which corresponds to an individual tetrahedral element size

of around 0.06 m near the fpv module. At mesh counts above 60000 (0.05 m), it varies much less.

Since these simulations took very long to compute, the less accurate $k-\varepsilon$ standard turbulence model was used for the computation. Even though a less accurate model was used, computational times of over 10 hours were recorded for simulating a flow time of 1 s. This was not feasible from a practical and resource standpoint and thus alternate forms of meshing like overset meshing was used with quadrilateral elements.

# D Wind Speed Calculations

The wind speed is calculated using the Harris spectral model. Equation D.1 describes the wind intensity definition using this model [12].

$$S_U(f) = \sigma_u^2 \frac{4 \cdot \frac{L_u}{U_{10}}}{\left(1 + 70.8 \cdot \left(\frac{fL_u}{U_{10}}\right)^2\right)^{5/6}} \tag{D.1}$$

Here,
$U_{10}$ is the 10-minute mean wind speed,
$S_U$ is the spectral density of the 10-minute mean wind speed,
$L_u$ is the integral length scale in m,
$\sigma_u$ is the standard deviation of wind speed in m/s,
$f$ is the values of positive sampled frequencies of the mean wind speed data.

Here, the values of $L_u$ and $\sigma_u$ are not standardised and have to be calculated. The integral length scale, $L_u$, describes the degree of turbulence in the flow. Lower length scales indicate smaller eddy formation and hence greater turbulence behaviour. The value of $L_u$ is calculated according to specifications in IEC 614001-1 [12] using the relation $L_u$ = 3.3 $z$. The equation is valid for height (z) ¡ 60 m, which is satisfied since the floater height is 0.42 m.

The variable $\sigma_u$ signifies the turbulence velocity of the flow. Since this is very complex to model, a mean turbulence velocity is assumed using the Equation D.2.

$$E\left[\sigma_U\right] = U_{10} \cdot A_x \cdot k_a \cdot \frac{1}{\ln \frac{z}{z_0}} = 0.43 \cdot U_{10} m/s, \quad A_x = \sqrt{4.5 - 0.856 \ln z_0} = 12.38 \tag{D.2}$$

where,
$E\left[\sigma_U\right]$ is the mean turbulence for a 10-minute resolution wind speed,
$k_a$ is the Von-Karman constant = 0.4,
$A_x$ is a constant depending on $z_0$,

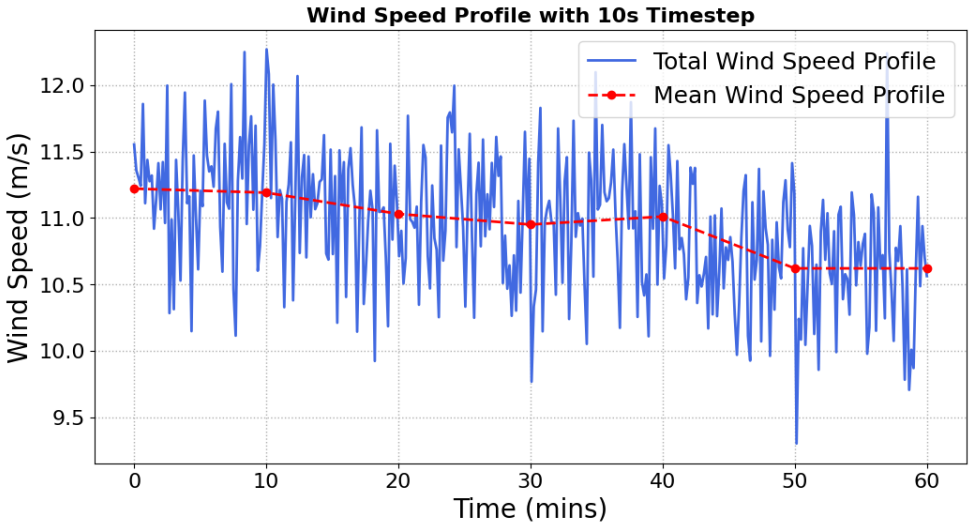


Figure D.1: Mean and complete wind speed profile of the PV yield study.

After determining the required parameters, the mean wind speed data needs to be converted to the frequency spectrum to condition the wind spectrum. A discrete Fourier transform is performed on the mean wind speed data to convert the data to a frequency spectrum. These values will then be applied to the mean wind speed data and conditioned. This data is then converted back to time-varying velocity using an inverse Fourier transform. The resulting wind speed data obtained is shown in Figure D.1.

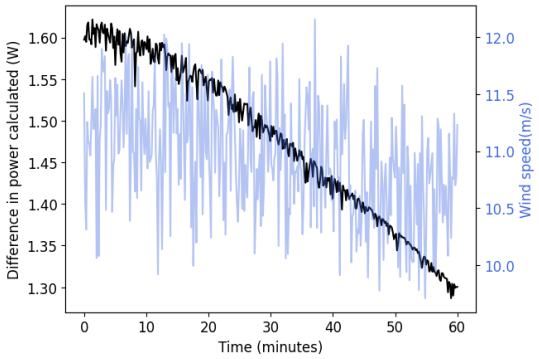


Figure D.2: Yield difference transposed with wind speed variation.

Based on the specifications available in Table 5.1, PV yield is calculated and it is found that only less than 1% of yield difference is identified with the inclusion of the tilt prediction model. The difference in yield is found to be between 1.3-1.6W and is transposed against the wind speed variation as shown in Figure D.2.

## Colophon

This document was typeset using LaTeX, using the KOMA-Script class `scrbook`. The main font is Palatino.